

NACA RM A53B16

6407

TECH LIBRARY KAFB, NM  
0143582



# RESEARCH MEMORANDUM

COMPARISON OF THE AERODYNAMIC CHARACTERISTICS AT  
TRANSONIC SPEEDS OF A PLANE WING AND A CAMBERED  
AND TWISTED WING, BOTH HAVING 45° OF SWEEPBACK  
AND AN ASPECT RATIO OF 6

By George H. Holdaway

Ames Aeronautical Laboratory  
Moffett Field, Calif.

Classification cancelled (or change to *Unclassified*)  
By authority of *Nasa Tech Pub Announcement # 125*  
(OFFICER AU REQUIRED TO CHANGE)  
*18 Mar 58*

By \_\_\_\_\_

*NK*

GRADE OF OFFICER MAKING CHANGE)

*27 Mar 61*

DATE

CLASSIFICATION

## NATIONAL ADVISORY COMMITTEE FOR AERONAUTICS

WASHINGTON

May 5, 1953

~~CONFIDENTIAL~~

*98/13*

~~CONFIDENTIAL~~

## NATIONAL ADVISORY COMMITTEE FOR AERONAUTICS

RESEARCH MEMORANDUMCOMPARISON OF THE AERODYNAMIC CHARACTERISTICS AT  
TRANSONIC SPEEDS OF A PLANE WING AND A CAMBERED  
AND TWISTED WING, BOTH HAVING  $45^\circ$  OF SWEEPBACK  
AND AN ASPECT RATIO OF 6

By George H. Holdaway

## SUMMARY

A transonic investigation was made by the free-fall technique of a plane wing and of a cambered and twisted wing, each having an aspect ratio 6, taper ratio of 0.5, and a sweepback of  $45^\circ$ . The wings were mounted on similar fuselage-tail combinations with fuselages of fineness ratio 12.4 and with tail surfaces swept back  $45^\circ$ . Measurements were made of the loads on the exposed wings, the pressures on the fuselage in the vicinity of the wing, and the acceleration and angle of attack of the complete model. Aerodynamic coefficients were determined for the two wings and for the complete model over a Mach number range of 0.86 to 1.08, with corresponding Reynolds numbers from 3,000,000 to 5,000,000, and over an angle-of-attack range of approximately  $0^\circ$  to  $12^\circ$ .

The results showed trends in agreement with wind-tunnel tests, and the use of camber and twist produced only slight changes in the lift and pitching-moment characteristics at transonic speeds. At low to moderate lift coefficients, the drag of the plane wing was, in general, less than that of the cambered and twisted wing. The cambered and twisted wing had lower drag coefficients at high lift coefficients for Mach numbers up to about 0.94. The wings and tails of both models were observed to be free from buffeting at lift coefficients up to about 0.4 throughout the test speed range.

## INTRODUCTION

Recent research investigations (refs. 1 and 2) revealed that the low-speed characteristics of a high-aspect-ratio  $45^\circ$  swept wing were improved at moderate to high lift coefficients by the incorporation of camber and twist. The more important improvements evidenced at these lift coefficients were a delay of the destabilizing variation in the

~~CONFIDENTIAL~~~~11-20-1951~~

pitching-moment curve to higher lift coefficients and a large reduction in drag. Significant improvements were also observed in the maximum lift coefficient and the lift-curve slope at large values of lift.

To determine whether these advantages extended to higher speeds, tests of reference 3 were made to cover the low to high subsonic speed range. The portion of these results, which corresponds to the Reynolds number and Mach number of references 1 and 2, was substantially in agreement with the prior tests. As the Mach number was increased to high subsonic speeds, however, the effectiveness of camber and twist in reducing the drag in the high lift-coefficient range and in improving the pitching-moment characteristics steadily deteriorated. At the highest test speeds, nearing the speed of sound, camber and twist actually had deleterious effects on the pitching moment. There was some question, however, as to whether this deterioration of the beneficial effects of camber and twist with increasing speed was entirely a Mach number effect, or an effect due to Reynolds number which decreased as the test Mach number was increased. The test data at a Mach number of 0.94 corresponded to a Reynolds number of 2,000,000, while the data at Mach number 0.25 were obtained at a Reynolds number of 10,000,000.

In an attempt to isolate the influences of Reynolds number and Mach number on the advantages or disadvantages of camber and twist at high subsonic speeds, the tests of reference 4 were made at Mach numbers of 0.6 to 0.9 with the Reynolds number increased to about 5,000,000. The results of these tests again showed that the camber and twist did not reduce the drag at high lift coefficients to the same degree as in references 1 and 2; however, the increased Reynolds number improved the pitching-moment characteristics to a degree where the cambered and twisted wing was only slightly inferior to the plain wing at the highest test speeds.

The tests of this report were undertaken to extend the investigation of the influence of camber and twist through the transonic speed range. Large-scale free-fall models were utilized as a means of traversing the transonic region. The tests covered a range of Mach numbers from 0.86 to 1.08 with corresponding Reynolds numbers of about 3,000,000 to 5,000,000. Supplementary data from these tests have been presented in references 5 and 6.

The models were dropped at Edwards Air Force Base, California under the supervision of personnel of the NACA from the Ames Aeronautical Laboratory.

## SYMBOLS

- A aspect ratio,  $\frac{b^2}{S}$
- a speed of sound, ft/sec
- $a_x$  longitudinal acceleration, units of g
- $a_z$  vertical acceleration, units of g
- b wing span measured perpendicular to plane of symmetry, ft
- $C_D$  drag coefficient for total configuration,  $\frac{\text{drag}}{q_0 S}$
- $C_{D_W}$  drag coefficient based upon exposed wing drag plus the drag component of pressure forces on fuselage in the vicinity of the wing,  $\frac{\text{drag}}{q_0 S}$
- $C_L$  lift coefficient for total configuration,  $\frac{\text{lift}}{q_0 S}$
- $C_{L_\alpha}$  lift-curve slope,  $\frac{\partial C_L}{\partial \alpha}$ , per deg
- $C_m$  pitching-moment coefficient for complete model about the model center of gravity,  $\frac{\text{pitching moment}}{q_0 S \bar{c}}$
- $C_{m_{\bar{c}/4}}$  wing pitching-moment coefficient about the lateral axis through the quarter-chord point of the total-wing mean aerodynamic chord,  $\frac{\text{pitching moment}}{q_0 S \bar{c}}$
- $C_{mq}$   $\frac{\partial C_m}{\partial (q \bar{c} / 2V)}$ , per radian
- $C_{m\dot{\alpha}}$   $\frac{\partial C_m}{\partial (\dot{\alpha} \bar{c} / 2V)}$ , per radian
- $\bar{c}$  total-wing mean aerodynamic chord,  $\frac{\int_0^{b/2} c^2 dy}{\int_0^{b/2} c dy}$ , ft
- c local wing chord measured parallel to plane of symmetry, ft

F	sum of spanwise concentrated loads applied along the elastic axis of a semispan wing panel, lb
g	acceleration of gravity, 32.2 ft/sec <sup>2</sup>
I	moment of inertia in pitch, slug-ft <sup>2</sup>
M	Mach number, $\frac{V}{a}$
m	concentrated couple applied near wing tip in a plane perpendicular to the quarter-chord line, in-lb
N	normal-force reading from wing balance system, lb
$P_l - P_u$	difference in static pressure between lower and upper surface at a fuselage station, lb/sq ft
q	pitching velocity, radians/sec
$\dot{q}$	$\frac{dq}{dt}$ , radians/sec <sup>2</sup>
$q_0$	dynamic pressure, $\frac{1}{2} \rho V^2$ , lb/sq ft
R	Reynolds number based upon $\bar{c}$
S	wing area, sq ft
$\frac{t}{c}$	airfoil-section thickness ratio, percent
V	free-stream velocity, ft/sec
$W_E$	weight of exposed wing panels, lb
y	spanwise coordinate normal to plane of symmetry, ft
$\Delta Z$	wing deflection normal to the XY plane
$\alpha$	angle of attack of longitudinal axis of model, deg
$\dot{\alpha}$	$\frac{d\alpha}{dt}$ , radians/sec
$\delta$	horizontal-tail deflection, deg
$\lambda$	ratio of wing tip chord to root chord at body center line

$\rho$  mass density of air, slugs/cu ft

$\theta$  angle of twist measured perpendicular to the quarter chord, radians

$\frac{\partial P}{\partial \alpha}$  load-coefficient slope,  $\frac{(P_l - P_u)_{\alpha_2} - (P_l - P_u)_{\alpha_1}}{(\alpha_2 - \alpha_1)q_0}$ , per deg

$\frac{\partial C_{m_{c/4}}}{\partial C_L}$  pitching-moment-coefficient slope

#### Subscripts

E aerodynamic coefficients ( $C_L$ ,  $C_D$ , and  $C_{m_{c/4}}$ ) based on exposed wing loads and total wing area

min minimum values

W aerodynamic coefficients ( $C_L$ ,  $C_m$ , and  $C_{m_{c/4}}$ ) based upon exposed wing loads plus component of load over fuselage in the vicinity of the wing and total wing area

#### MODEL

Two fuselages of fineness ratio 12.4, each with four tail surfaces swept back  $45^\circ$ , were used in the test program. The plane wing and the cambered and twisted wing were interchanged between fuselages during the course of the tests. A drawing of these wings, fuselages, and the tail surfaces is presented in figure 1, and a photograph of the model with the skin removed and the recovery dive brake open is shown in figure 2.

The wings were similar in that they had the same taper ratio of 0.5, aspect ratio of 6, sweepback of  $45^\circ$ , were constructed of solid 24 ST aluminum alloy, and were mounted on the fuselages with  $0^\circ$  dihedral and  $-0.17^\circ$  incidence. Both wings had airfoil sections defined normal to the quarter-chord line but differed in that one wing, identified as the plane wing, had symmetrical NACA 64A010 airfoil sections, while the cambered and twisted wing had NACA 64A810 airfoil sections (cambered for design  $C_{L_w} = 0.4$ ). The latter wing was also twisted uniformly in a streamwise direction  $-10^\circ$  between fuselage center line and tip chords.

The wings were mounted on two lift beams and two drag torsion beams in a wing balance system as shown in figure 3. The juncture between the wing and the fuselage skin was sealed with a fold of rubber (cemented to

~~CONFIDENTIAL~~

the wing) which permitted relatively unrestricted wing movement in respect to the fuselage skin.

The vertical-tail surfaces were operated differentially during the free-fall to provide roll-position stabilization. The horizontal-tail surfaces were activated together in accordance with a preset schedule to adjust the model trim attitude and to provide intermittent controlled disturbances in pitch. Both the vertical- and horizontal-tail surfaces were all movable and pivoted about axes perpendicular to the model center line.

#### INSTRUMENTATION

NACA continuously recording flight instruments were used to record the various quantities listed below:

<u>Quantity</u>	<u>Instrument</u>
Angle of attack and angle of sideslip	Slave selsyn or recording oscillograph (depending upon installation) recording movements of vane mounted on boom ahead of body (figs. 1 and 2)
Vertical and longitudinal accelerations	Strain-gage-type linear accelerometer with recording oscillograph and NACA three-component accelerometer
Transverse acceleration	NACA three-component accelerometer
Angular acceleration in pitch	Strain-gage-type angular accelerometer with recording oscillograph
Rate of roll and pitch	NACA turnmeter
Horizontal- and vertical-tail deflections	NACA two-component control-position recorder
Mach number, dynamic pressure, and sixteen differential pressures	Three NACA six-cell manometers

The wing balance used to measure the exposed-wing loads consisted primarily of strain-gage bridge circuits with the sensing elements located on three support members, as shown in figure 3. Strain gages

on both the top and the bottom of each of the two lift beams were connected together in a balanced bridge circuit. The drag member was supported by two fixed shafts on which were mounted torsion strain gages wired as another balanced bridge circuit. The rolling and yawing moments of the wing panels were resisted by eight thrust bearings which also maintained the wing in proper alinement.

Wing-tip deflections were recorded in flight with a 16-millimeter motion picture camera which was mounted within the fuselage at the center of the root chord, and was sighted along the 50-percent-chord line and focused at the wing tip. Calibrations made before the flights permitted the reading of the projected photographs in inches of wing-tip deflection.

The pressure differences between the top and bottom surfaces of the fuselage were measured at orifice locations along the body center line and at positions rotated  $45^\circ$  to the left of center, from body station 76.5 to station 116. The orifice locations are shown in figure 4.

The airspeed system was calibrated at different angles of attack through the Mach number range using the SCR 584 radar installation of the NACA High-Speed FLight Research Station at Edwards Air Force Base.

All the flight records were synchronized by means of a chronometric timer.

## TESTS

### Flight-Test Procedure

The models were released from a carrier airplane (fig. 5) at altitudes of 40,000 to 42,000 feet and allowed to fall freely without propulsion. During the first portion of the test drop, the model was trimmed at approximately zero angle of attack to provide minimum drag and hence maximum speed. When the desired Mach number was reached the horizontal stabilizer was moved abruptly in accordance with a preset schedule to a new trim position, and from this position the control was pulsed periodically at 2.4-second intervals to produce an oscillatory disturbance of about  $\pm 4^\circ$  about the trim angle of attack. The wing data presented herein were obtained from an analysis of the entire record taken during the oscillations produced by each pulse. The complete model data were analyzed only in the regions between pulses where the horizontal control surfaces were stationary. The series of pulses was terminated at a calculated time which would provide a safe altitude for recovery. The envelope of the curves of Reynolds number variation with Mach number during the complete oscillatory period of the tests is shown in figure 6.

## Wing Aeroelasticity Tests

In addition to the flight measurements of wing-tip deflections, laboratory measurements were made with the wings loaded statically using spanwise distributions obtained from low-speed wind-tunnel tests reported in reference 2, and the twist and deflection due to various bending and torsion moments were recorded.

## PRECISION OF MEASUREMENTS

Based upon instrument precisions and their effect on the computed coefficients, the estimated incremental error of any one reading is believed to be within the values listed below:

Item	Estimated maximum incremental error	
	M = 0.85	M = 1.05
$C_L$	$\pm 0.02$	$\pm 0.009$
$C_{L_E}$ and $C_{L_W}$	$\pm 0.02$	$\pm 0.008$
$C_D$	$\pm 0.002$	$\pm 0.001$
$C_{D_E}$ and $C_{D_W}$	$\pm 0.006$	$\pm 0.002$
$C_m$	$\pm 0.009$	$\pm 0.004$
$C_{m_c/4_E}$ and $C_{m_c/4_W}$	$\pm 0.005$	$\pm 0.002$
Mach number	$\pm 0.01$	$\pm 0.01$
Angle of attack	$\pm 1/4^\circ$	$\pm 1/4^\circ$

## EVALUATION OF DATA

## Exposed Wing

The first step in the process of data reduction was to plot as time histories the lift, drag, and pitching-moment coefficients for the exposed wing panels. The values of  $C_{L_E}$ ,  $C_{D_E}$ , and  $C_{m_c/4_E}$  for constant integer angles of attack were read from the time histories and plotted as a function of Mach number. By this method of analyzing the data, any differences between the increasing and decreasing values would appear in the Mach number cross plots as scatter in the data. These differences could be due to difficulty in making precise time correlation between records, in evaluating instrument lag characteristics, or due to

aerodynamic lag. For the flight tests during which the angle-of-attack oscillations were small, there was very little scatter in the data and the errors were well within the listed instrument accuracies. When the rate of pitch was large, the technique caused errors with the sign and magnitude dependent on the direction and rate of pitch. These errors were not sufficiently consistent to evaluate; therefore, values of the coefficients obtained from faired curves similar to those of figure 7 were used to determine the faired data curves. Figure 7 presents typical results for a number of drops of each wing for one angle of attack.

#### Fuselage Loads in Vicinity of Wing

The pressure-load-coefficient slopes  $\partial P/\partial\alpha$  were obtained for each pair of orifices. These slopes were first integrated spanwise with a parabolic distribution and then integrated chordwise to obtain  $\partial C_L/\partial\alpha$  and  $\partial C_M/\partial\alpha$ . Data from reference 5 for the same fuselage without a wing showed that the fuselage loads approached zero at the wing location, so that in the present investigation the loadings could, with little error, be considered as due entirely to the wing.

The drag contribution of the fuselage in the vicinity of the wing was approximated by assuming it equal to the product of the normal pressure loading and the sine of the angle of attack. This procedure would give the drag rise with angle of attack with reasonable accuracy, but would underestimate the contribution of the fuselage elements to the minimum drag of the wing, since this procedure would provide no pressure drag at zero angle of attack and also would neglect friction drag.

#### Total-Wing Characteristics

The loads and moments for the fuselage in the vicinity of the wing were added to those for the exposed wing to obtain the characteristics that have been identified as those of the complete or total wing.

#### Total-Model Characteristics

Lift, drag, and pitching-moment coefficients of the complete model were calculated from the acceleration data, plotted as time histories, and faired for constant angles of attack in the same manner as for the exposed-wing loads. The method used in the computation of the pitching

moment of the complete model about its center of gravity is presented in appendix A. As before, the mean values of the coefficients were used to determine the final data curves, except that the drops with different stabilizer settings were evaluated separately.

### Aeroelasticity Corrections

Due to the fact that the aeroelastic effects noted during the laboratory measurements were very nearly the same for both wings, no significant effect on the comparison of the wings would be anticipated. Hence, no corrections were made to the data. The results and discussion of the aeroelasticity tests are included in appendix B.

### RESULTS

Data curves faired as in figure 7 were used as the basis for the cross plots which were drawn through all points determined for constant integer angles of attack. The variations of lift, drag, and pitching moment at various Mach numbers for the exposed wing are presented in figure 8 for both the plane wing and the cambered and twisted wing. All the coefficients are based on a total-wing area which includes the area inside the fuselage bounded by the extension of the leading and trailing edges to the plane of symmetry.

In figure 9, the fuselage loading distribution  $\partial P/\partial \alpha$  in the vicinity of the wing is presented for both wings as a function of chord-wise fuselage stations for various Mach numbers. Data are presented for orifices along the fuselage center line and the  $45^\circ$  line.

The aerodynamic coefficients for the total wing are presented in figure 10 at various Mach numbers.

The lift coefficients for both configurations of the complete model are shown in figure 11 as a function of angle of attack for different Mach numbers and stabilizer settings.

The drag coefficients for the complete model are plotted in figure 12 as a function of lift coefficient at different Mach numbers. To remove the effect of differences in stabilizer settings from the comparisons, data are presented for only one stabilizer setting,  $\delta = -4^\circ$ , with corresponding trim lift coefficients as noted on the curves of figure 12. The drag-data presentation is limited to only one model fuselage to eliminate observed differences in drag which appeared attributable to differences in model details.

Presented in figure 13 are the pitching-moment coefficients of the complete model about its center-of-gravity location for various Mach numbers. The pitching-moment data for the total wing, presented earlier, were converted to moments about the model center of gravity and included in this figure so that comparisons could be made more readily.

## DISCUSSION

In the ensuing discussion certain variations are discussed as principally an effect of changing Mach number. It should be borne in mind that limitations of the test technique result in unavoidable variation of Reynolds number with Mach number (see fig. 6). There is evidence (refs. 3 and 4) that some of the factors discussed are sensitive to Reynolds number as well as Mach number changes. Where the effects of Reynolds number are particularly significant, the results are discussed in relation to the Reynolds number. However, in those instances where the discussion does not specifically relate the observed effects to changes in Reynolds number, it should be realized that the influence of Reynolds number may still be present in the results.

### Lift

The lift curves for exposed wing, complete wing, and total model (figs. 8(a), 10(a), 11(a), and 11(b)) are of conventional character. The curves are relatively linear at small angles of attack ( $\alpha < 6^\circ$ ) for all Mach numbers. Above an angle of attack of  $6^\circ$  the curves tend to decrease slope by various amounts, depending upon the Mach number, the wing tested, and the portion of the wing or fuselage being considered.

Lift-curve slope.- The lift-curve slopes presented in figure 14, taken at angles of attack where  $C_{LW} = 0.4$ , show that for both wings values of  $C_{L\alpha}$  and  $C_{L\alpha W}$  increase with Mach number up to  $M = 0.94$  and thereafter decrease. The values of  $C_{L\alpha W}$  for the plane wing were greater than those for the cambered and twisted wing, about half this difference being attributed to a change in loading over the fuselage.

There is indicated a greater difference between  $C_{L\alpha}$  of the total wing and of the complete model for the plane wing than for the cambered and twisted wing. Inasmuch as this difference between wing and model is probably due primarily to the tail, then a lower downwash slope is indicated for the plane wing. This lower downwash for the plane wing appears consistent with the greater wing-tip deflections for the plane wing (see appendix B and fig. 24) which indicated a greater outboard distribution

of spanwise loading. The greater deflection of the plane wing was not due to lesser rigidity, because laboratory tests indicated that the cambered and twisted wing had essentially the same stiffness as the plane wing.

Comparison of the lift-curve slopes with wind-tunnel data (fig. 14) shows reasonably good agreement for the plane wing and for the cambered and twisted wing at a Mach number of 0.86. For the cambered and twisted wing at Mach numbers above 0.86, there was a progressive departure between the flight and wind-tunnel data.

Maximum lift.- The maximum lift coefficients for the wings, that is, the lift coefficients corresponding to the peak of the lift curve, were not reached in the present investigation. However, as noted in reference 7, the lift coefficient obtained in flight corresponding to initial stall is defined by the coefficient at a break in the lift-curve slope rather than the coefficient corresponding to maximum lift. The pitching-moment results to be discussed later verify that for these models destabilizing changes in pitching moment occur at the lift coefficients at which the lift-curve slope decreases. These destabilizing changes in pitching moment, associated with the onset of the stall, will be discussed in the section Pitching-Moment Characteristics at High Lift Coefficients.

#### Pitching Moment of Wings

The curves of pitching-moment coefficient  $C_{m\bar{c}}/4$  plotted against lift coefficient (figs. 8(b) and 10(b)) are reasonably linear at the lower lift coefficients; however, both wings show destabilizing variations at the higher lift coefficients, particularly at the lower Mach and Reynolds numbers.

Pitching-moment characteristics at low lift coefficients.- The values of the slopes for the two wings up to moderate lift coefficients are quite similar, with the aerodynamic center moving from values of 50 to 53 percent of  $\bar{c}$  at a Mach number of 0.9 to 60 percent  $\bar{c}$  at Mach number 1.06. The aerodynamic centers are at least 20 percent  $\bar{c}$  rearward from the location of 30 percent  $\bar{c}$  indicated by subsonic theory (ref. 8).

Pitching-moment characteristics at high lift coefficients.- The variations of the pitching-moment coefficient for the complete wing with lift coefficient are characterized by destabilizing variations (initial stall) at high lift coefficients, particularly at the lower Mach numbers. The camber and twist was effective in delaying the destabilizing change in the pitching-moment curve to a higher lift coefficient for Mach numbers

from 0.98 to 1.06 with accompanying Reynolds numbers of 4 to 5 million. For the Mach numbers less than 0.98, camber and twist caused the destabilizing variation to occur at slightly lower lift coefficients, but the severity of the change was less with camber and twist than for the plane wing.

The data of reference 4 showed that increasing the Reynolds number of the tests resulted in an increase in the lift coefficient at which a destabilizing variation in pitching moment occurred for the cambered and twisted wing, but Reynolds number had only a small effect on the characteristics of the plane wing. Based on this knowledge, the lower lift coefficients for the cambered and twisted wing as compared with the plane-wing flight data, for Mach numbers less than 0.98, were probably due to the effect of reduced Reynolds numbers on the cambered and twisted wing. Reasonable agreement was noted at similar Reynolds numbers between flight and tunnel data for the Mach number variation of the lift coefficient for the onset of the destabilizing variation of the pitching moment.

#### Pitching Moment of Complete Model

It is of interest to note in figure 13 that the relatively large variations in the pitching-moment data for the total wings at Mach number 0.94 were also evident in the data for the complete model, but the variations occur at slightly different angles of attack.

Also presented in figure 13 are straight lines representing  $\partial C_m / \partial \alpha$  based upon the same tests as this report but computed from the periods of stick-fixed oscillations as reported in reference 6. The slopes of the pitching-moment-coefficient curves for the complete model as obtained from reference 6 appear to be in good agreement with the average slopes from the evaluations of this report (appendix A).

The data of figure 13 confirm the fact that, in general, the pitching-moment coefficients for the cambered and twisted wing are slightly more linear than those for the plane wing over a larger angle-of-attack range.

#### Drag

The effect of Mach number on the drag characteristics of the two wings based on total-wing data at various lift coefficients is presented in figure 15. For the lower lift coefficients ( $C_L = 0$  through 0.2) the drag of the plane wing was less than that of the cambered and twisted

wing through the Mach number range as shown in figure 15. At lift coefficients of 0.4 to 0.6, however, the relative drags were dependent upon the Mach number, the drag of the cambered and twisted wing being less up to a Mach number of about 0.94 and greater above this Mach number.

The differences in the total-wing drag between the two wings at the higher lift coefficients are confirmed qualitatively by the data for the complete model shown in figure 12. The magnitude of the differences for the complete model are, however, greater than those for the total wing. Because the differences for the complete model are intimately related to the model configuration, the complete model results are not considered generally applicable.

The total-wing drag coefficients for both wings are lower than the values presented in references 3 and 4, particularly at low lift coefficients. Some of this difference can be attributed to the fact that the total-wing drag coefficients of this investigation were calculated neglecting pressure drag at zero angle of attack and friction drag for the portion of the wing included within the fuselage.

Figure 16 presents for several Mach numbers a comparison between the experimental curves of drag due to lift for the two wings and theoretical drag-rise curves for full leading-edge suction and no leading-edge suction. The test data for both wings approach their respective curves of drag due to lift for no leading-edge suction.

#### Buffet Boundaries

Figure 17 shows a typical oscillograph record from which the buffet boundaries were deduced. The intensity of the buffet was not sufficient to have a marked effect on the  $a_z$  record; therefore, the wing-balance lift records were used primarily in the analysis. The maximum oscillation of the  $a_z$  record due to buffeting was 0.2 g (not shown in fig. 17). The magnitude of this acceleration is small in comparison to the total range of accelerations, but is a significant value for buffet of airplanes. It is of interest to note that the buffet frequency was approximately 20 cps which was constant for both wings throughout the Mach number range of the tests. This frequency corresponds to the first bending frequency of the body and is quite different from the wing and instrument natural frequencies of 38 and 95 cps, respectively. The persistency of the vibration is typical of many buffet records.

With the horizontal tail located directly in line with the wing-chord plane, it was to be expected that the wake from the wing might produce tail fluctuations. Vibrations superimposed upon the control-position records were interpreted as possible tail buffet. The only

time the records indicated tail buffet was during periods of wing buffet and of body vibrations following wing buffet. Thus at low lift coefficients where the tail presumably is close to the center line of the wing wake, no buffeting was apparent on the tail surfaces.

The total-wing lift coefficients at which apparent buffeting of the wing was first observed for the two wings are presented in figure 18. As was indicated in references 9 and 10, present methods for predicting the buffet boundaries for swept wings are inadequate, and attempts to analyze the data for the wings of this report in similar manner were unsatisfactory. It was observed, however, that there was a similarity between the buffet boundaries and the lift coefficients at the point of destabilizing variation in the  $C_{m_c}/4$  curve.

A conclusion which can be seen easily from the data of figure 18 is that there is a range of lift coefficients from 0.05 to 0.35 for which the wing, and consequently the tail, were entirely free of buffet at all the transonic speeds tested. The lift coefficients for the buffet boundary for the cambered and twisted wing at the lower Mach numbers would probably be increased for higher test Reynolds numbers on the order of 4,000,000 or greater.

#### CONCLUSIONS

A comparison of data from flight tests at transonic speeds of a plane wing and a cambered and twisted wing of the same plan form has resulted in the following conclusions with regard to the wings tested:

1. Camber and twist produced only slight changes in the lift and pitching-moment characteristics of the plan form tested.
2. At low to moderate lift coefficients, the drag of the plane wing was, in general, less than that of the cambered and twisted wing throughout the speed range of the tests. The drag advantage of the cambered and twisted wing at high lift coefficients, which was established in all the previous investigations at low and high subsonic speeds, was observed in this investigation to exist up to a Mach number of about 0.94. At speeds above this value the plane wing exhibited the lesser drag.
3. The wings and tails of both models were observed to be free from buffeting at total-wing lift coefficients up to about 0.4 throughout the test speed range. The lift coefficients at which the initiation of buffet

~~CONFIDENTIAL~~

was observed agreed approximately with the lift coefficients corresponding to the point of destabilizing variation in the wing pitching-moment curves.

Ames Aeronautical Laboratory  
National Advisory Committee for Aeronautics  
Moffett Field, Calif.

~~CONFIDENTIAL~~

## APPENDIX A

METHOD USED IN COMPUTING  $C_m$ 

The pitching-moment coefficient for the complete model was computed using the following expression:

$$C_m = \frac{I\dot{q}}{q_0 S \bar{c}} - C_{m_q} \frac{q\bar{c}}{2V} - C_{m_{\dot{\alpha}}} \frac{\dot{\alpha}\bar{c}}{2V}$$

where  $q$  and  $\dot{q}$  were measured directly, and  $\dot{\alpha}$  was computed from the relationship

$$\dot{\alpha} = q - \frac{32.2 (a_z - 1)}{V}$$

The values of  $C_{m_q}$  and  $C_{m_{\dot{\alpha}}}$  were assumed to have the variations with Mach number as shown in figure 19. The variations in figure 19 were estimated by an approximate separation of the values of  $C_{m_q} + C_{m_{\dot{\alpha}}}$  given in reference 6.

## APPENDIX B

## AEROELASTICITY TESTS

Laboratory measurements were made of the wing deflections under load with the exposed wing panels held rigid at the line of intersection of wings with the fuselage. Couples were applied at the wing tip to simulate wing twisting moments, and from the recorded wing twist the elastic axis of each wing was determined and is presented in figure 20(a). The characteristics of each wing in pure bending were determined by applying loads to the wing along the elastic axis. The spanwise load distribution was obtained from low-speed experiments presented in reference 2. Figure 20(b) shows how a 1500-pound bending load was distributed at six loading points on the elastic axis in accordance with the spanwise distributions given in reference 2 for a lift coefficient of 0.8 (tests were also made for 500- and 1000-lb loads per panel).

In determining the elastic axes, the torsional stiffness parameter  $\theta/m$  was also determined for each wing and is shown in figure 21. The magnitude of this parameter was found to be small and, hence, its effect on the test data was not evaluated.

The bending-stiffness parameter per unit load is presented in figure 22, and the resultant geometric twist in a streamwise direction due to the bending deflections of the wing for positive lift is presented in figure 23.

A comparison of the wing-tip deflections photographed in flight with the deflections measured in the laboratory tests is presented in figure 24. The tip deflections of the plane wing were generally greater than those of the cambered and twisted wing; this is particularly evident at the higher Mach numbers ( $M = 0.99$  to  $1.08$ ). The flight deflection data indicate that, as the Mach number was increased, the center of loading tended to move outboard.

The effect of the aeroelastic twist of the wings on the lift-curve slope and the shift in the aerodynamic-center location was computed utilizing equations (6), (8), and (10a) of reference 8 and values of twist due to bending at four spanwise stations from figure 23 for a net load of 1500 pounds per panel. The computed effective angle of attack at the root chord required to give zero lift for the negative twist angles was  $1.87^\circ$  for the plane wing and  $1.83^\circ$  for the cambered and twisted wing. The computed  $C_{m_0}$  due to the wing deflections for  $C_{LW} = 0.8$  was 0.0127 for the plane wing and 0.0119 for the cambered and twisted wing. When a lift-curve slope of 0.08 is used for both wings, the effect on the lift-curve slope is an increase of approximately 18.5 percent from the flexible-wing data to the rigid-wing case. Similarly, the aerodynamic

center of the plane wing would be shifted rearward 1.59 percent of the mean aerodynamic chord in converting the flexible-wing data to the rigid-wing case and 1.49 percent for the cambered and twisted wing.

## REFERENCES

1. Hunton, Lynn W.: Effects of Twist and Camber on the Low-Speed Characteristics of a Large-Scale  $45^\circ$  Swept-Back Wing. NACA RM A50A10, 1950.
2. Hunton, Lynn W., and Dew, Joseph K.: The Effects of Camber and Twist on the Aerodynamic Loading and Stalling Characteristics of a Large-Scale  $45^\circ$  Swept-Back Wing. NACA RM A50J24, 1951.
3. Johnson, Ben H., Jr., and Shibata, Harry H.: Characteristics Throughout the Subsonic Speed Range of a Plane Wing and of a Cambered and Twisted Wing, Both Having  $45^\circ$  of Sweepback. NACA RM A51D27, 1951.
4. Shibata, Harry H., Bandettini, Angelo, and Cleary, Joseph W.: An Investigation Throughout the Subsonic Speed Range of a Full-Span and a Semispan Model of a Plane Wing and of a Cambered and Twisted Wing, All Having  $45^\circ$  of Sweepback. NACA RM A52D01, 1952.
5. White, Maurice D., and Look, Bonne C.: Load Distribution Over a Fuselage in Combination With a Swept Wing at Small Angles of Attack and Transonic Speeds. NACA RM A51E15, 1951.
6. White, Maurice D.: Effect of Camber and Twist on the Stability Characteristics of Models Having a  $45^\circ$  Swept Wing as Determined by the Free-Fall Method at Transonic Speeds. NACA RM A52F16, 1952.
7. Spreiter, John R., and Steffen, Paul J.: Effect of Mach and Reynolds Numbers on Maximum Lift Coefficient. NACA TN 1044, 1946.
8. DeYoung, John, and Harper, Charles W.: Theoretical Symmetric Span Loading at Subsonic Speeds for Wings Having Arbitrary Plan Form. NACA Rep. 921, 1948.
9. Purser, Paul E., and Wyss, John A.: Review of Some Recent Data on Buffet Boundaries. NACA RM L51E02a, 1951.
10. Gadeberg, Burnett L., and Ziff, Howard L.: Flight-Determined Buffet Boundaries of Ten Airplanes and Comparisons With Five Buffeting Criteria. NACA RM A50I27, 1951.

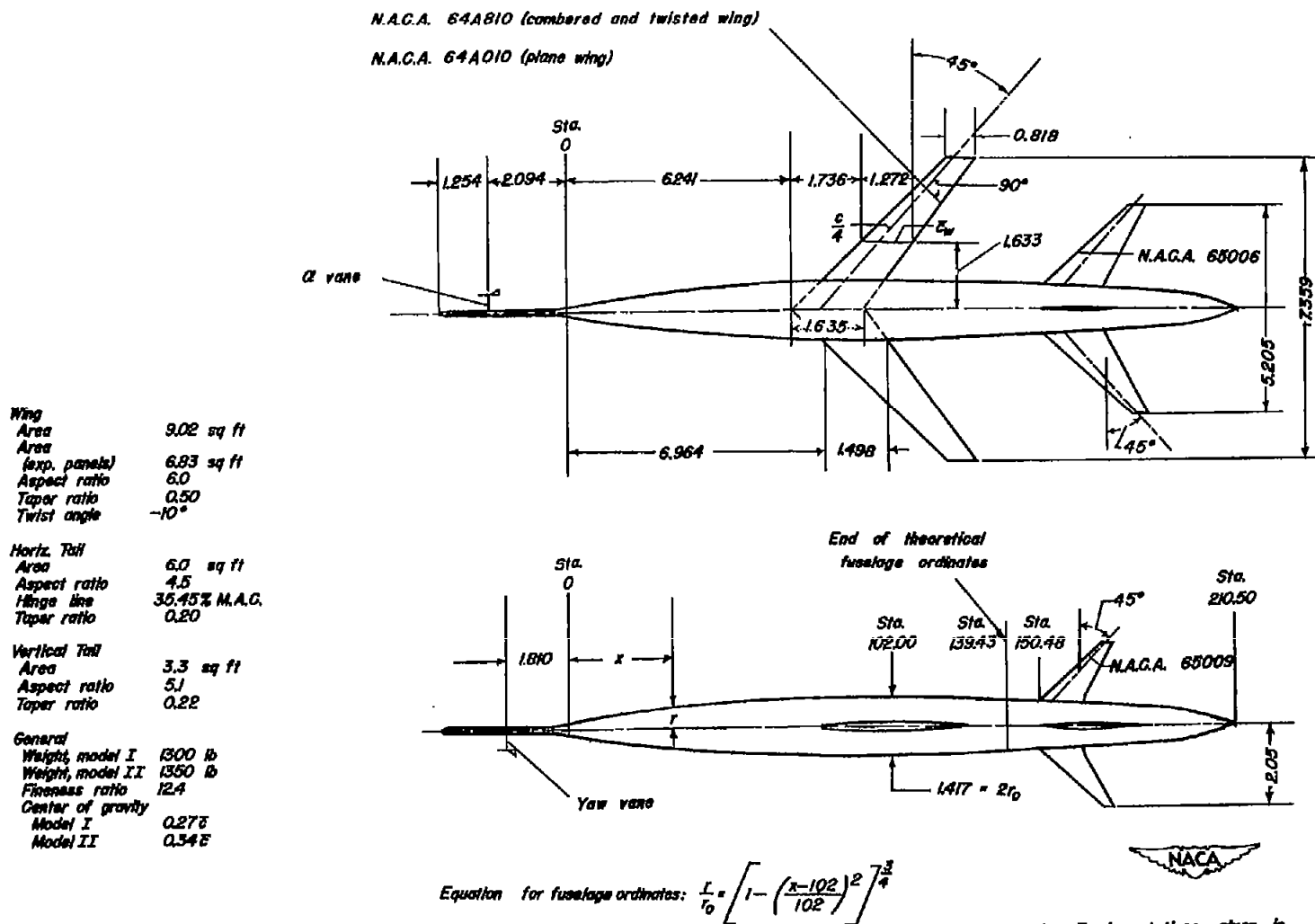


Figure 1. - Dimensional sketch of test model configuration.



Figure 2.- Free-fall model with skin removed and  
dive brake open

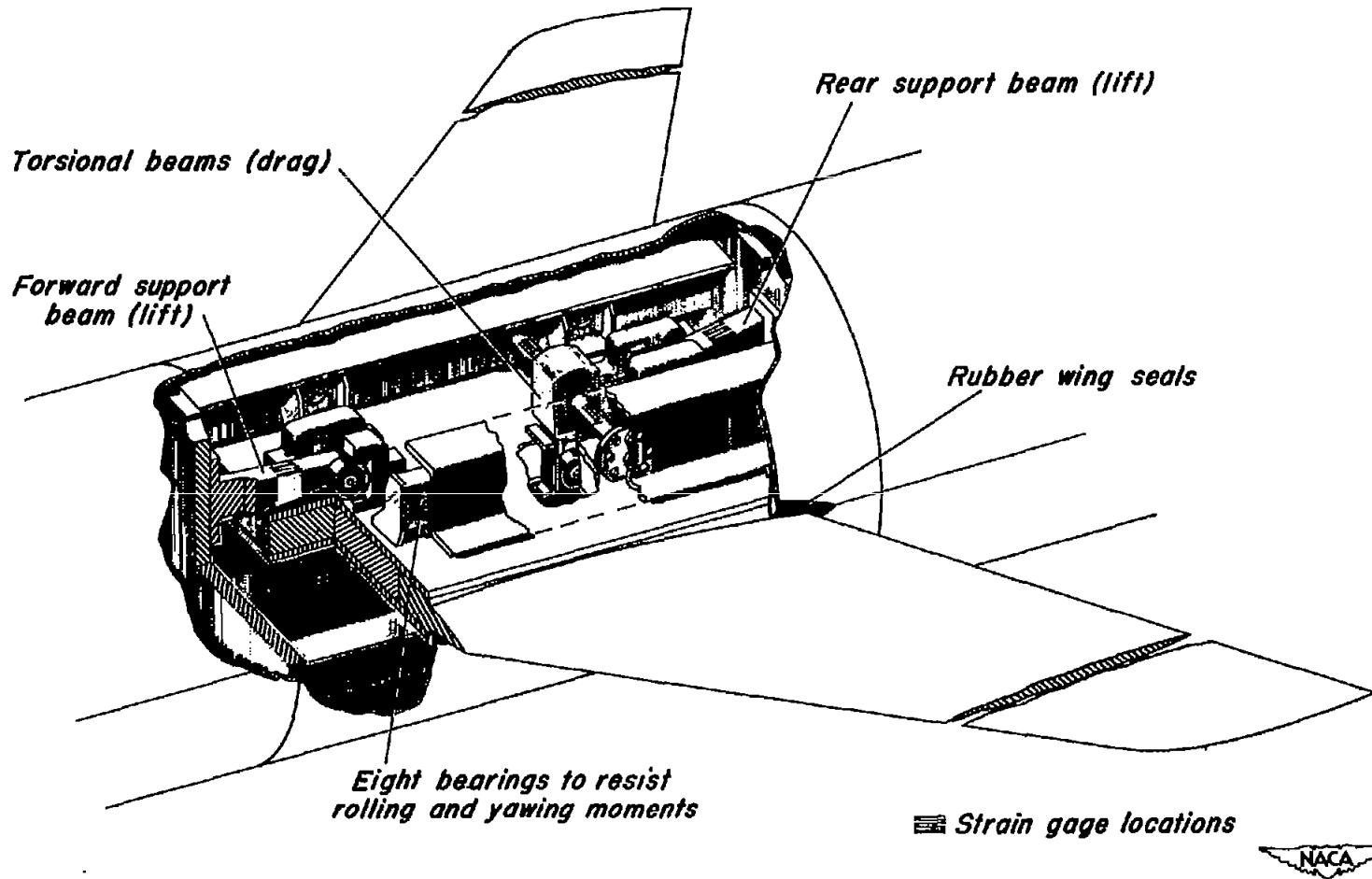


Figure 3.- Balance system for measuring exposed wing forces of lift, drag, and pitching moment.

All 45° orifices are on left side of fuselage  
except lower-surface orifice at station 107.5

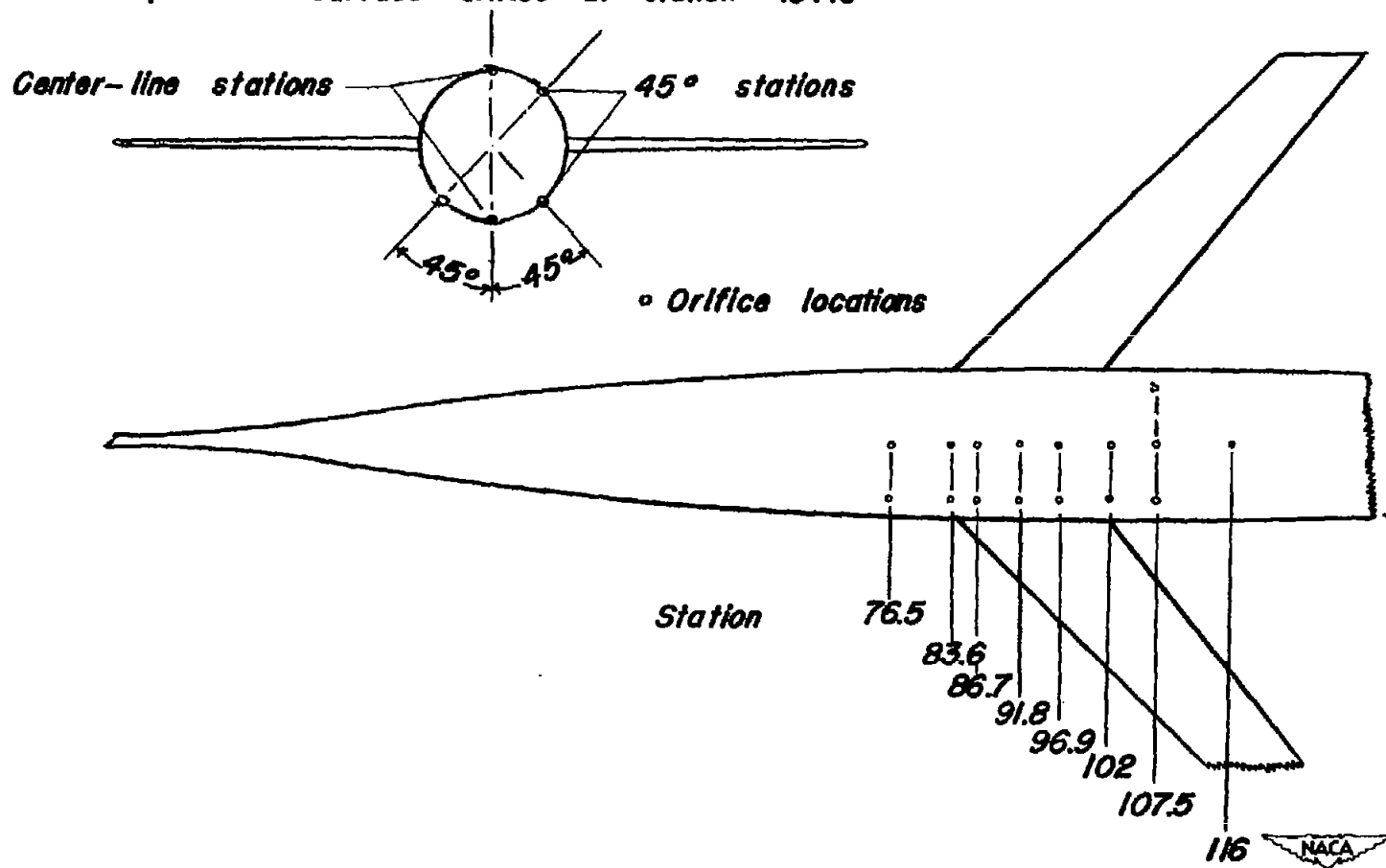


Figure 4.— Locations of pressure orifices on upper and lower surfaces of fuselage.

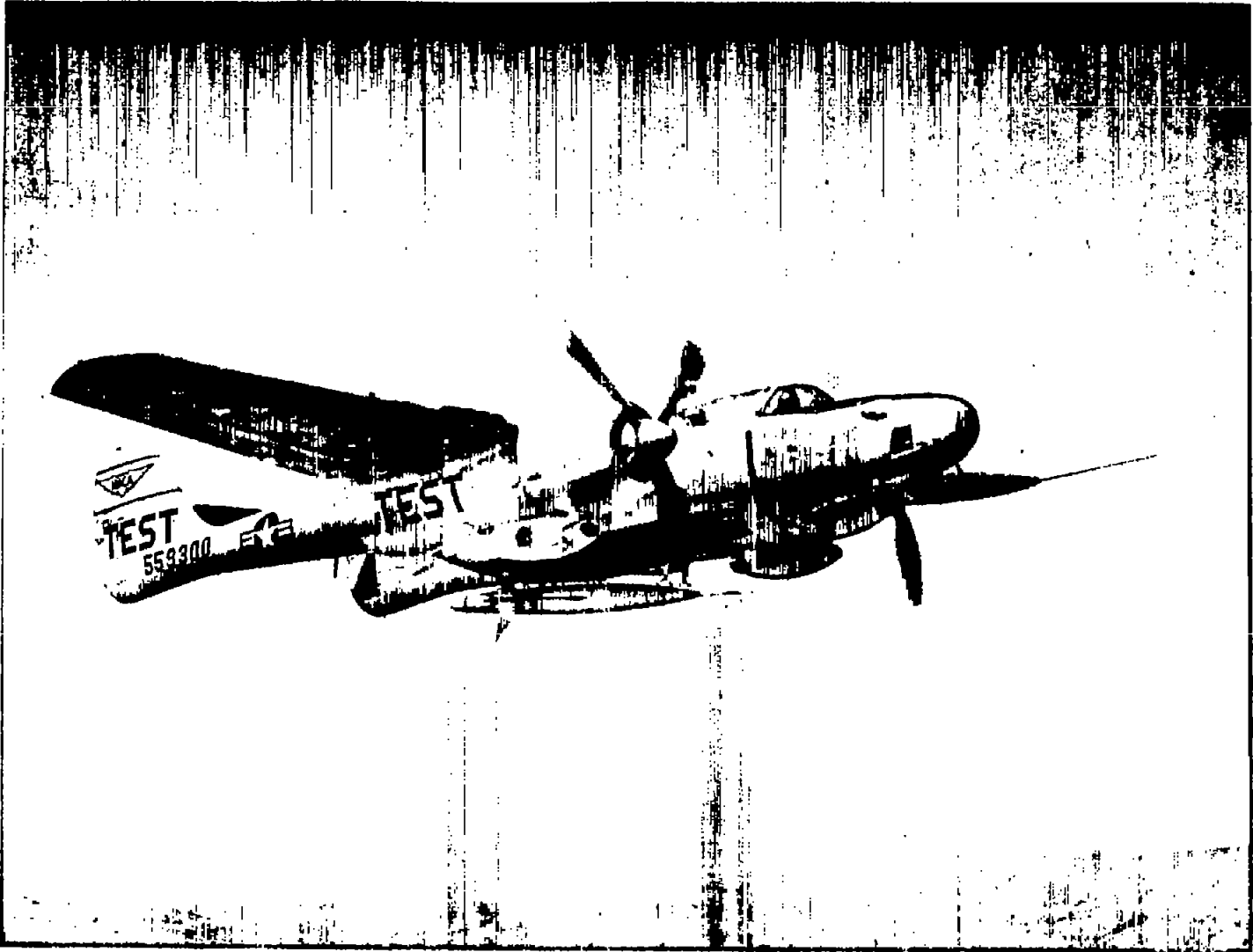


Figure 5.- Free-fall model mounted on carrier airplane.

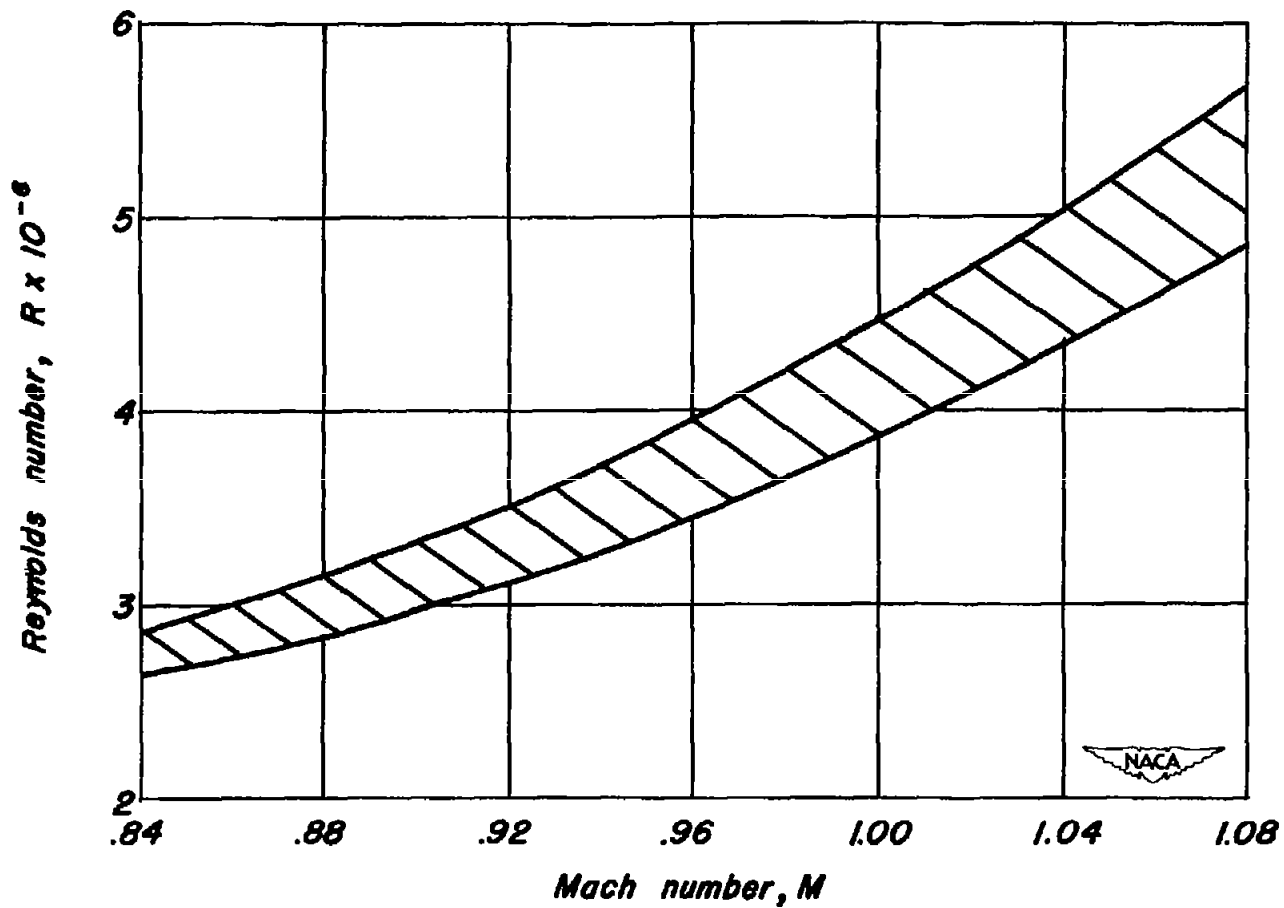
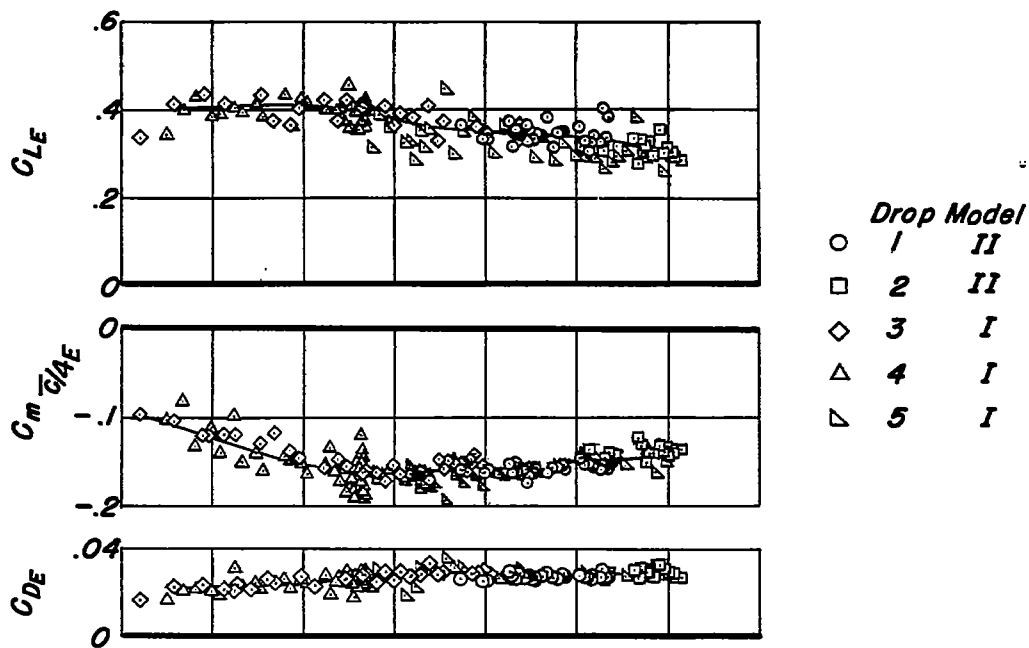
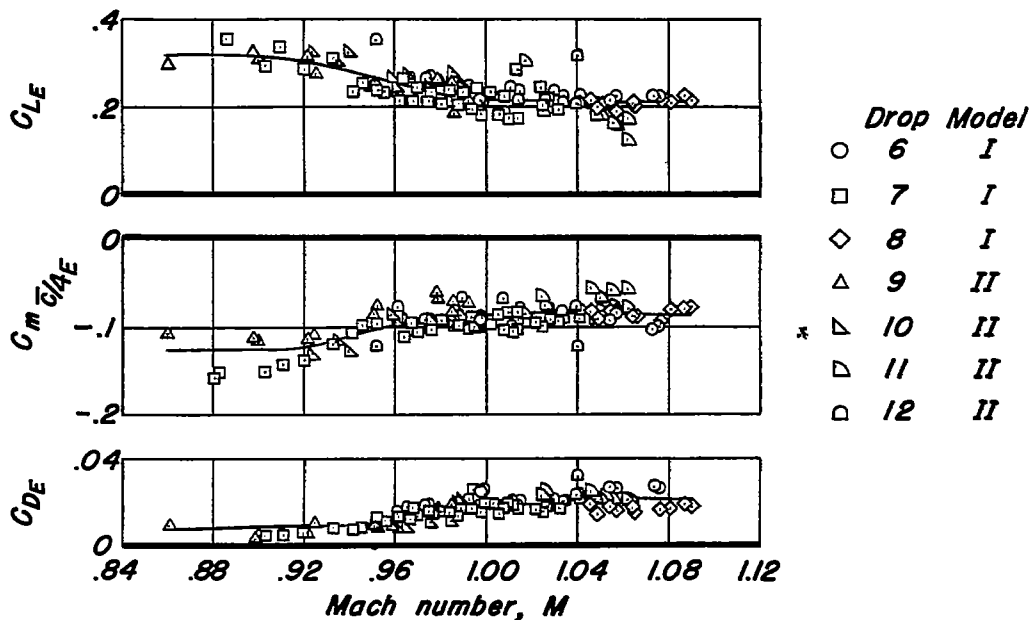


Figure 6.— Envelope of Reynolds number variation with Mach number for the series of tests.



(a) Plane wing.



(b) Cambered and twisted wing.



Figure 7. - Typical plot of data points used in obtaining faired curves of aerodynamic characteristics based upon exposed-wing loads (angle of attack, 5°).

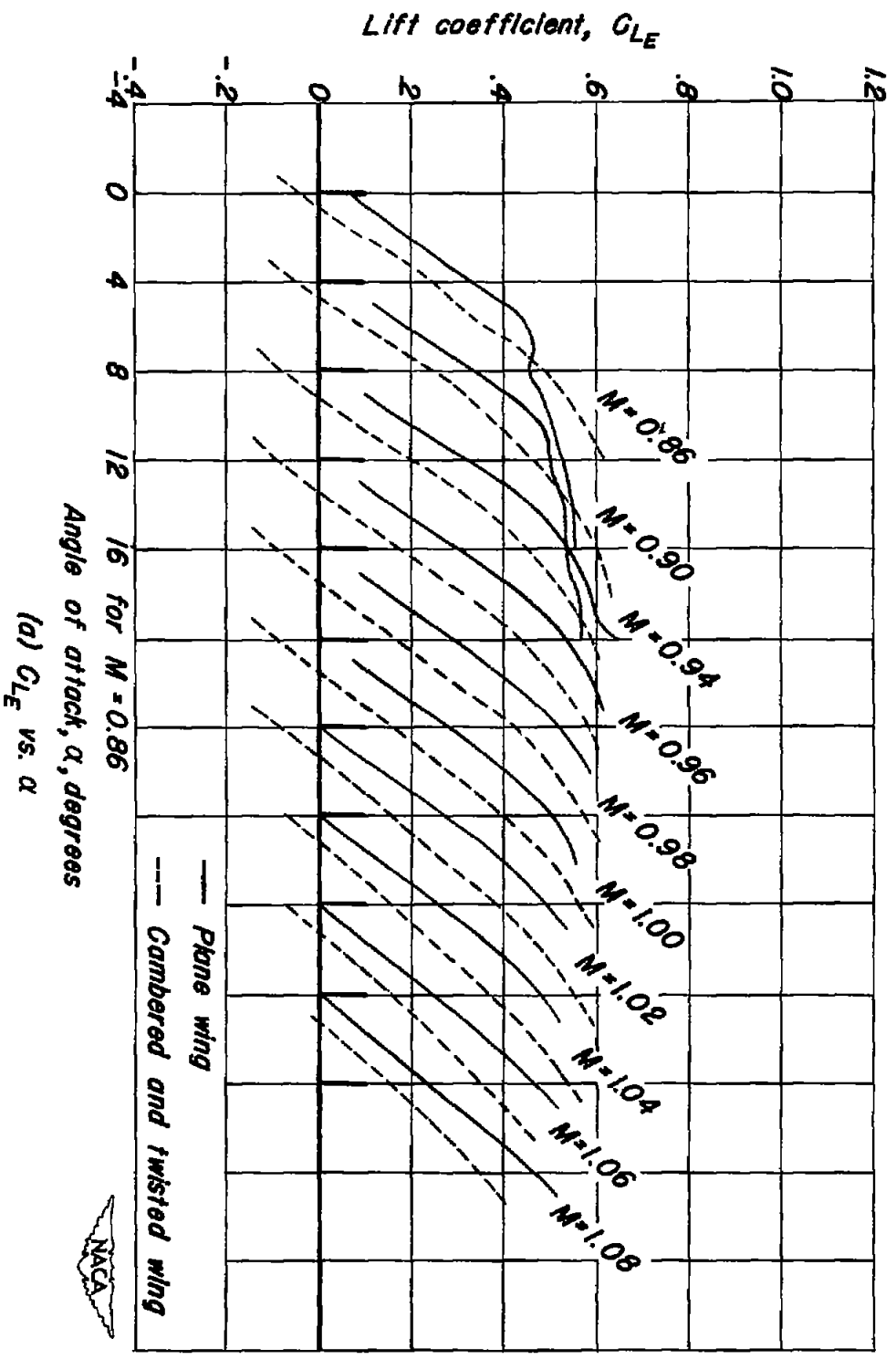


Figure 8.— The aerodynamic characteristics for the two wings at various Mach numbers, based upon exposed—wing loads and total—wing area.

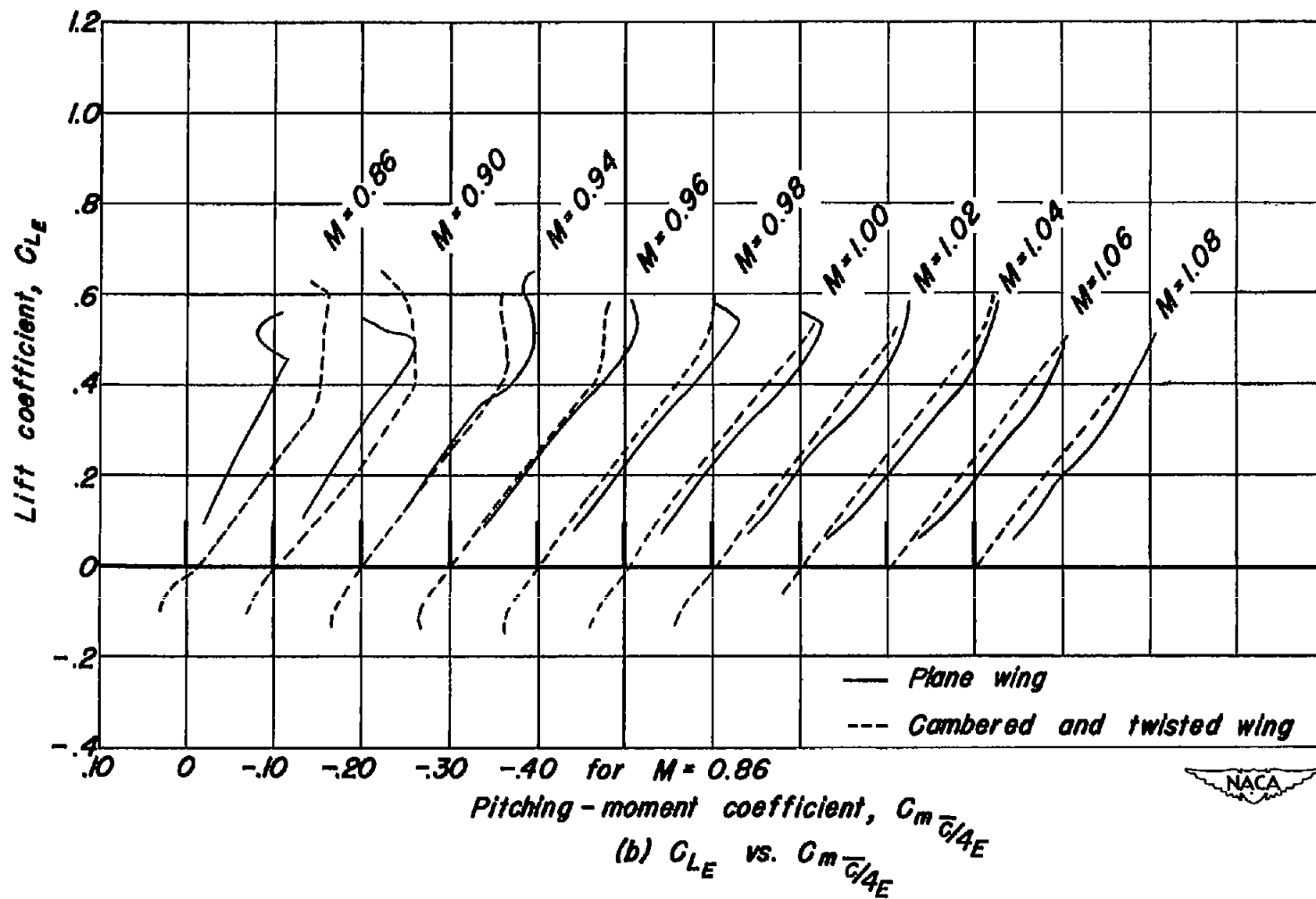


Figure 8.- Continued.

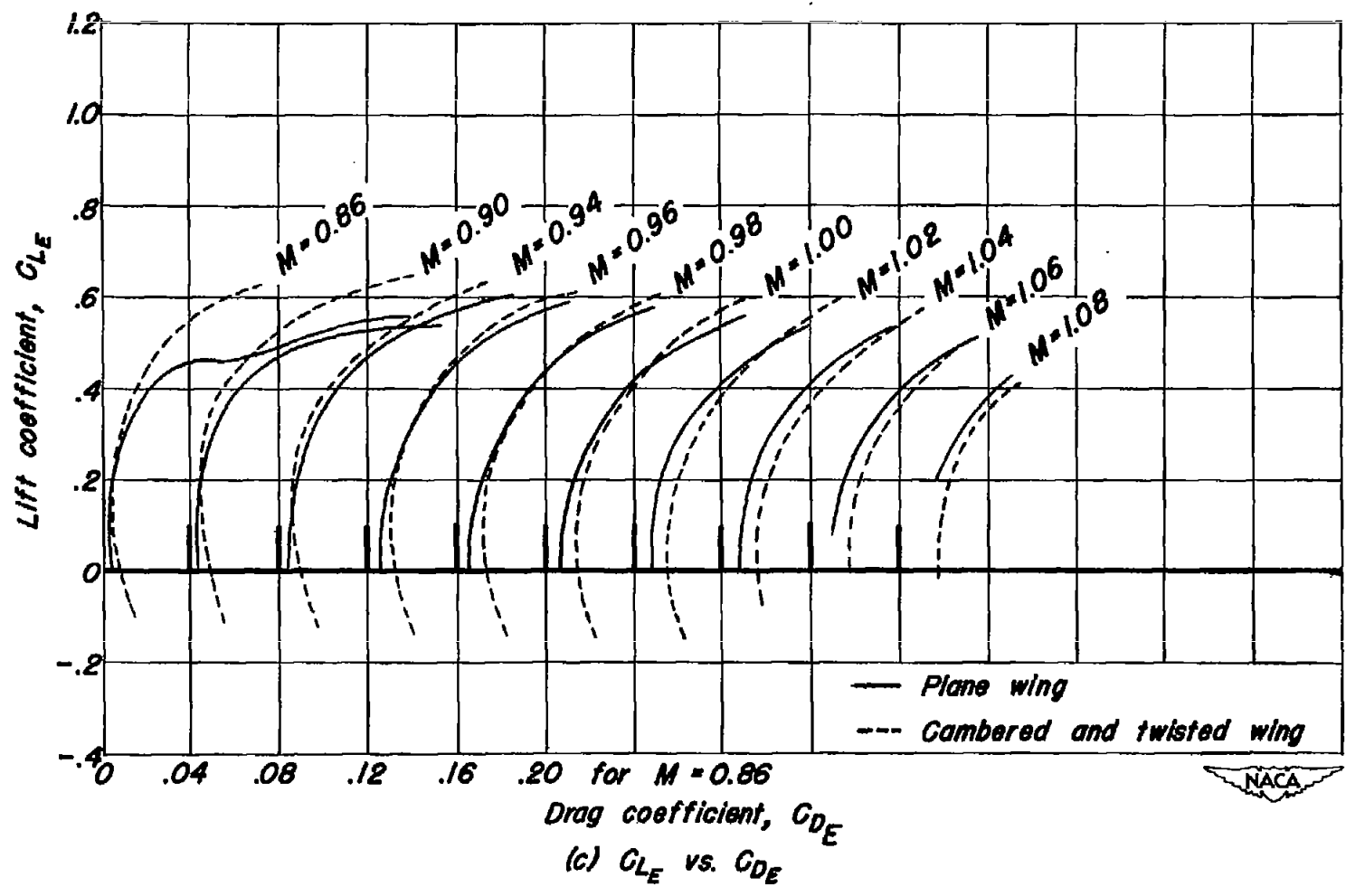


Figure 8.- Concluded.

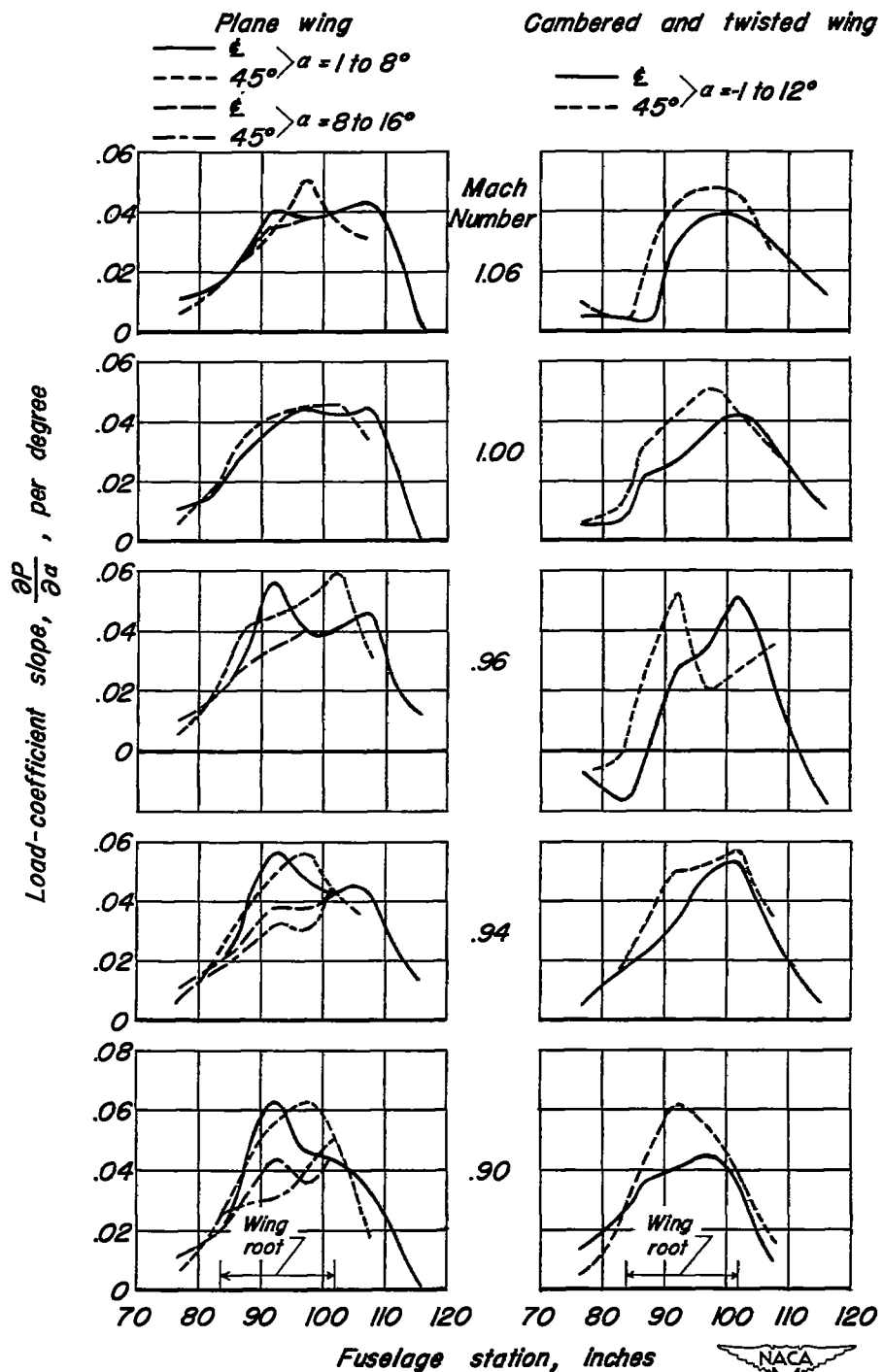


Figure 9.— Chordwise distributions of load-coefficient slope over fuselage in vicinity of wing at various Mach numbers.

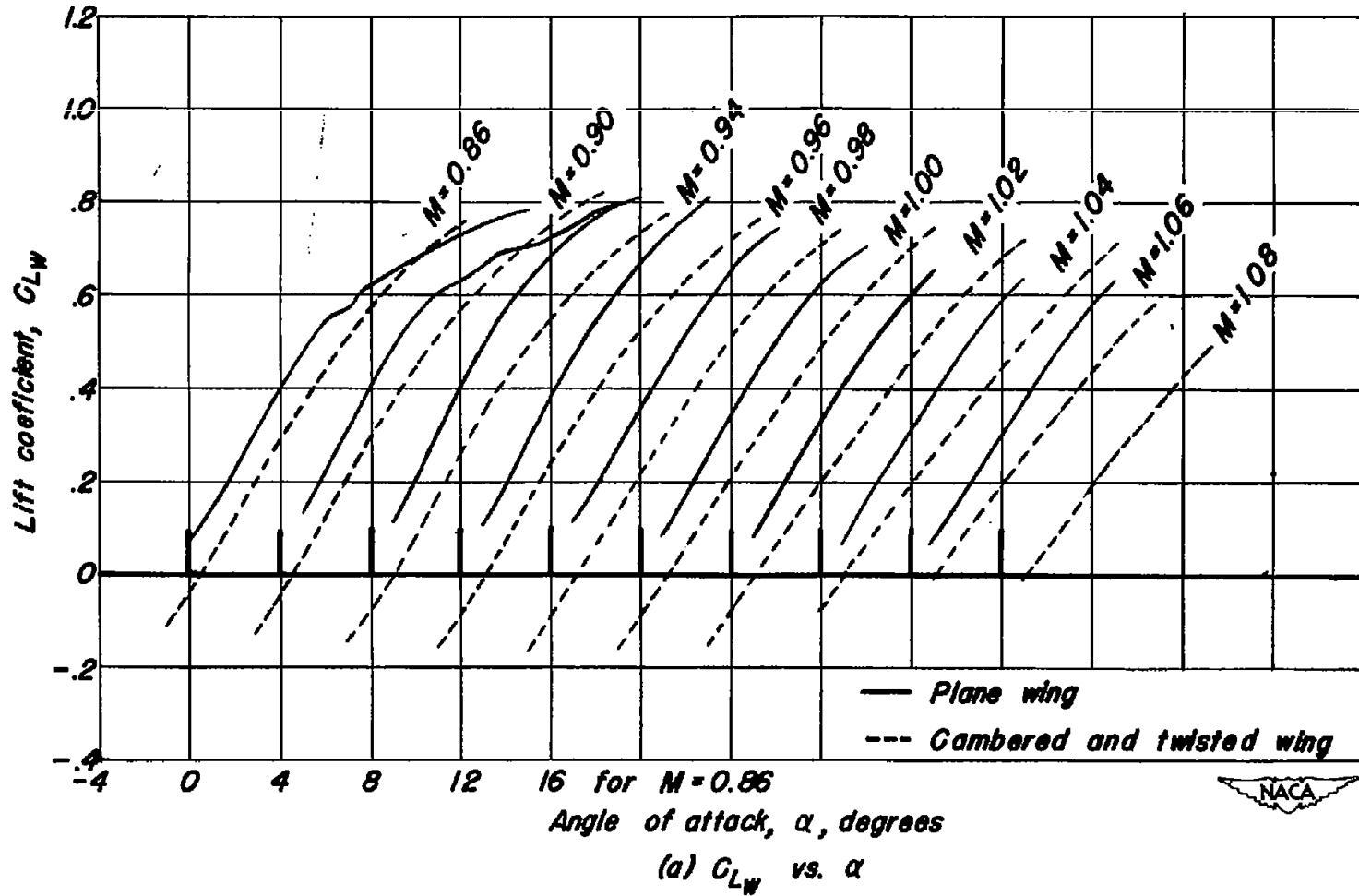


Figure 10.— The aerodynamic characteristics of the two wings at various Mach numbers, based upon exposed-wing loads plus load over fuselage in vicinity of the wing.

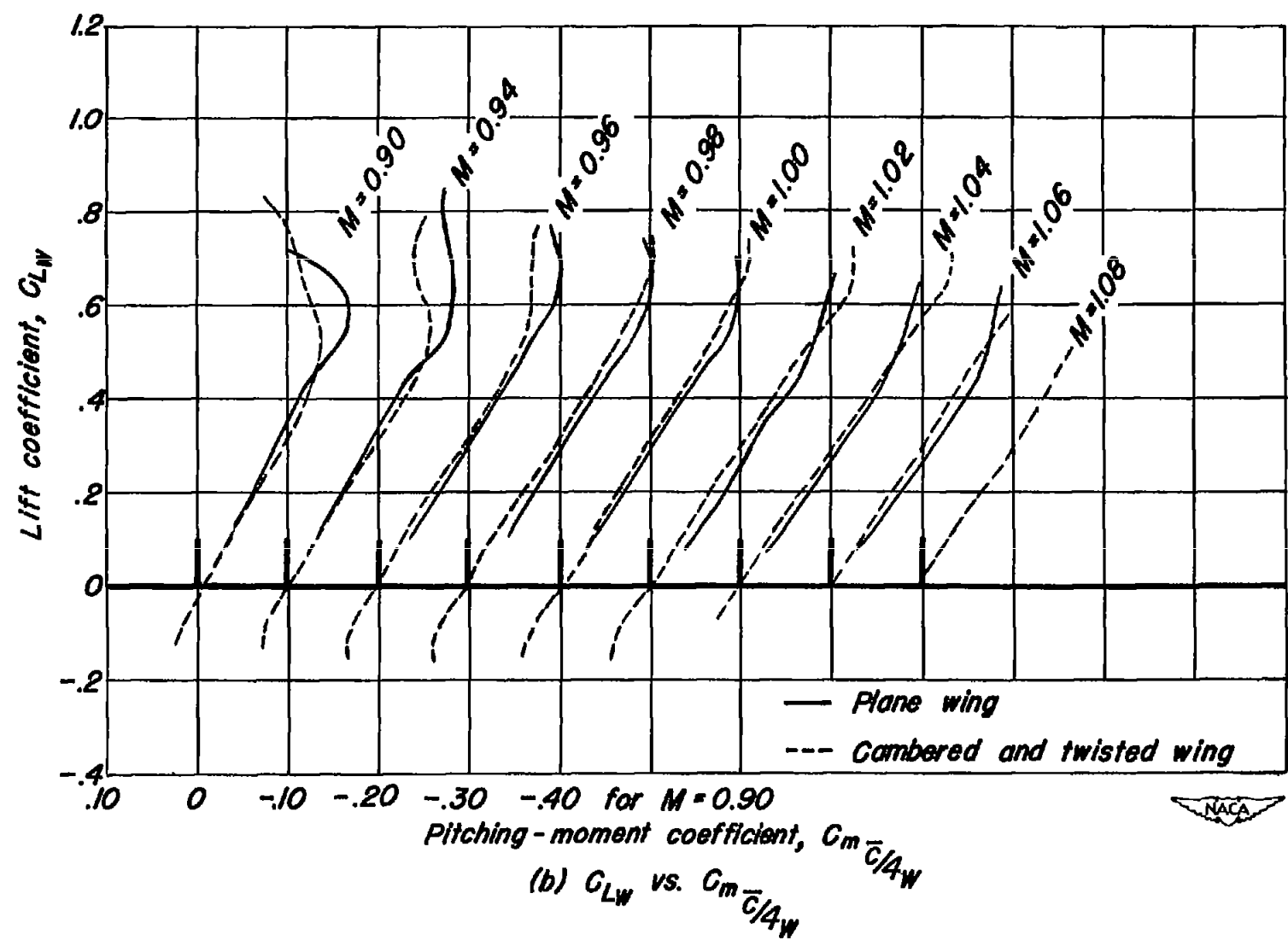
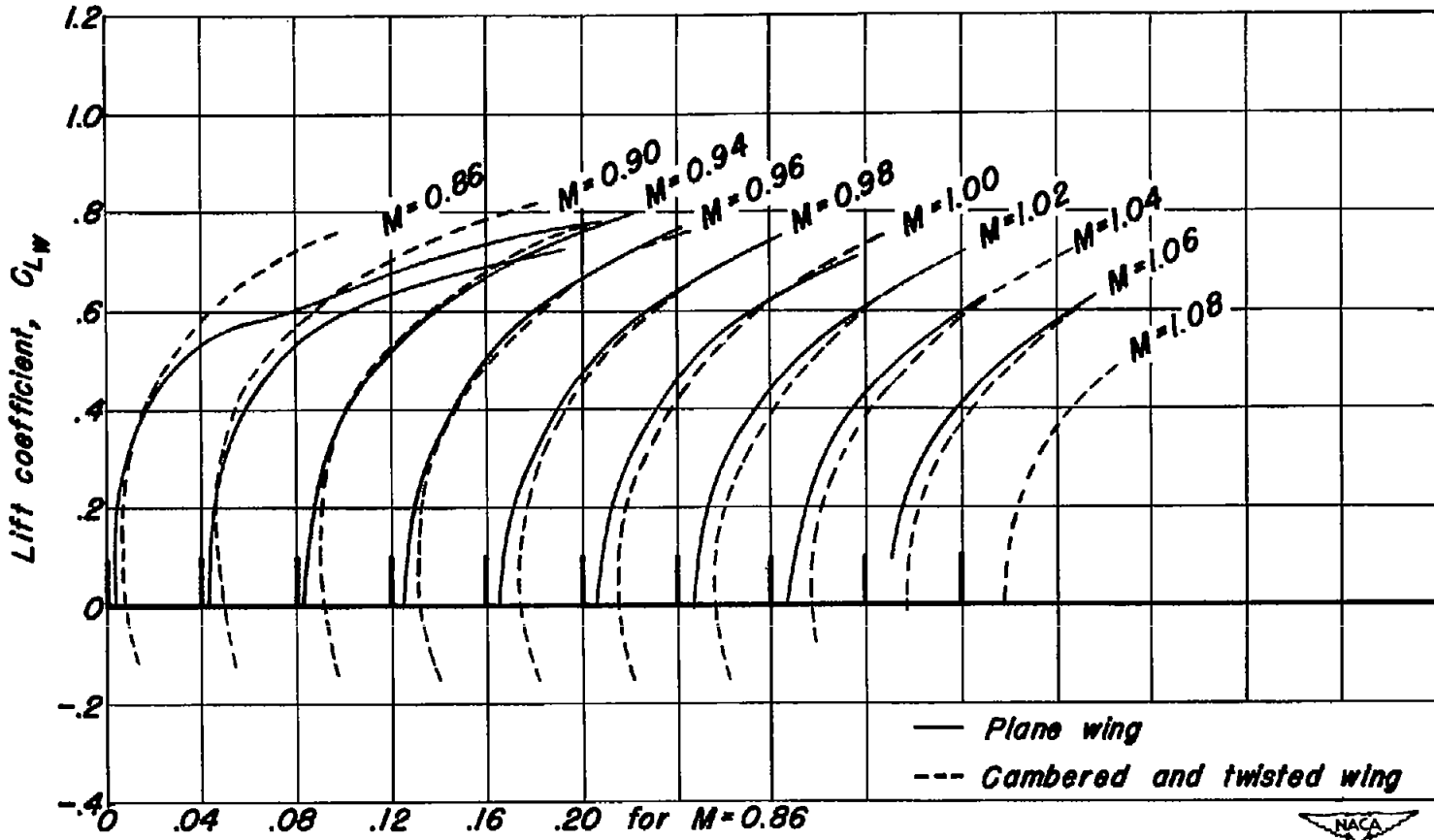
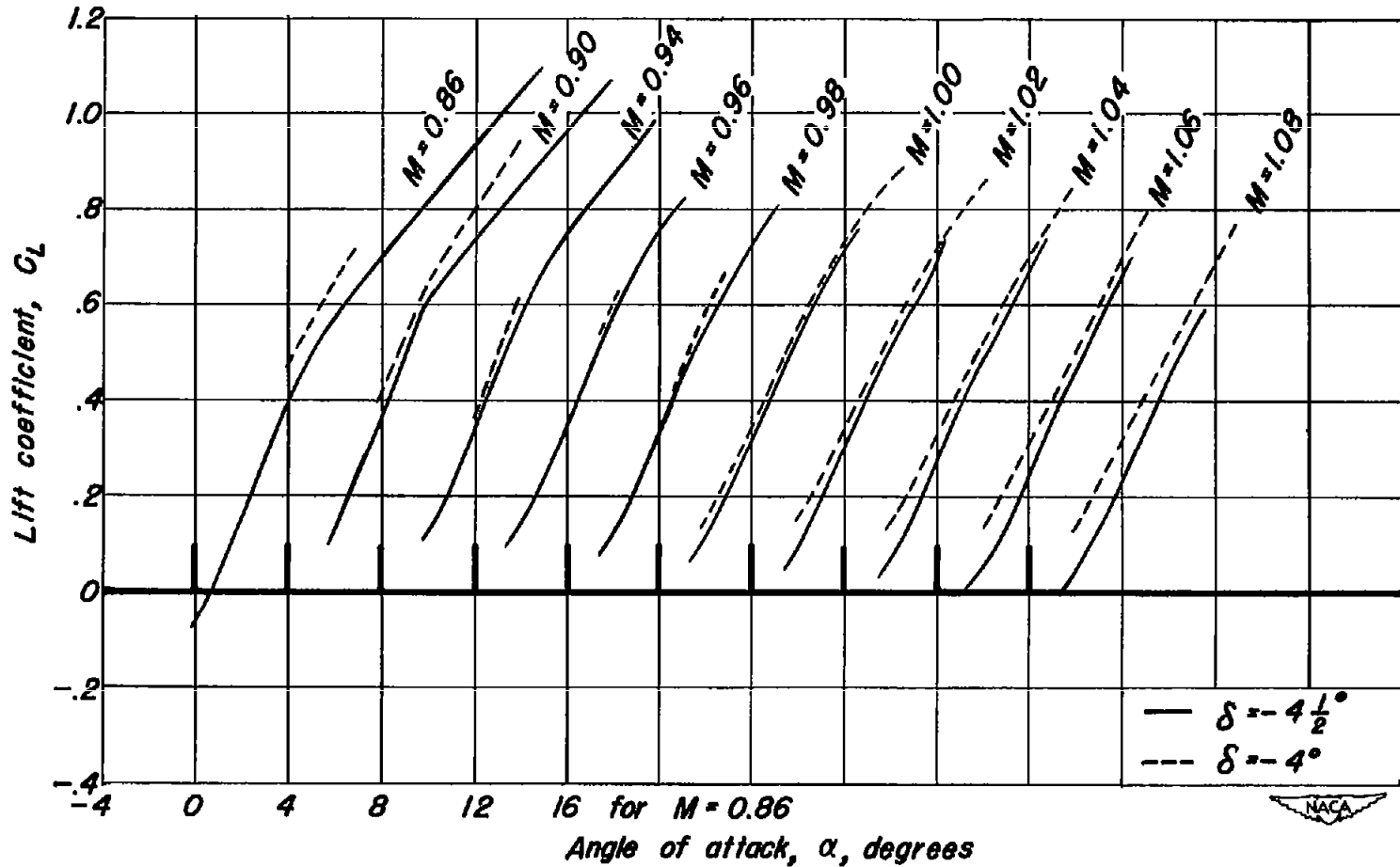


Figure 10.— Continued.



Drag coefficient,  $C_{DW}'$   
(c)  $C_{LW}$  vs.  $C_{DW}'$

Figure 10. - Concluded.



(a) Plane wing.

Figure 11.— The lift coefficients of the complete model at various Mach numbers, for different horizontal stabilizer settings,  $\delta$ .

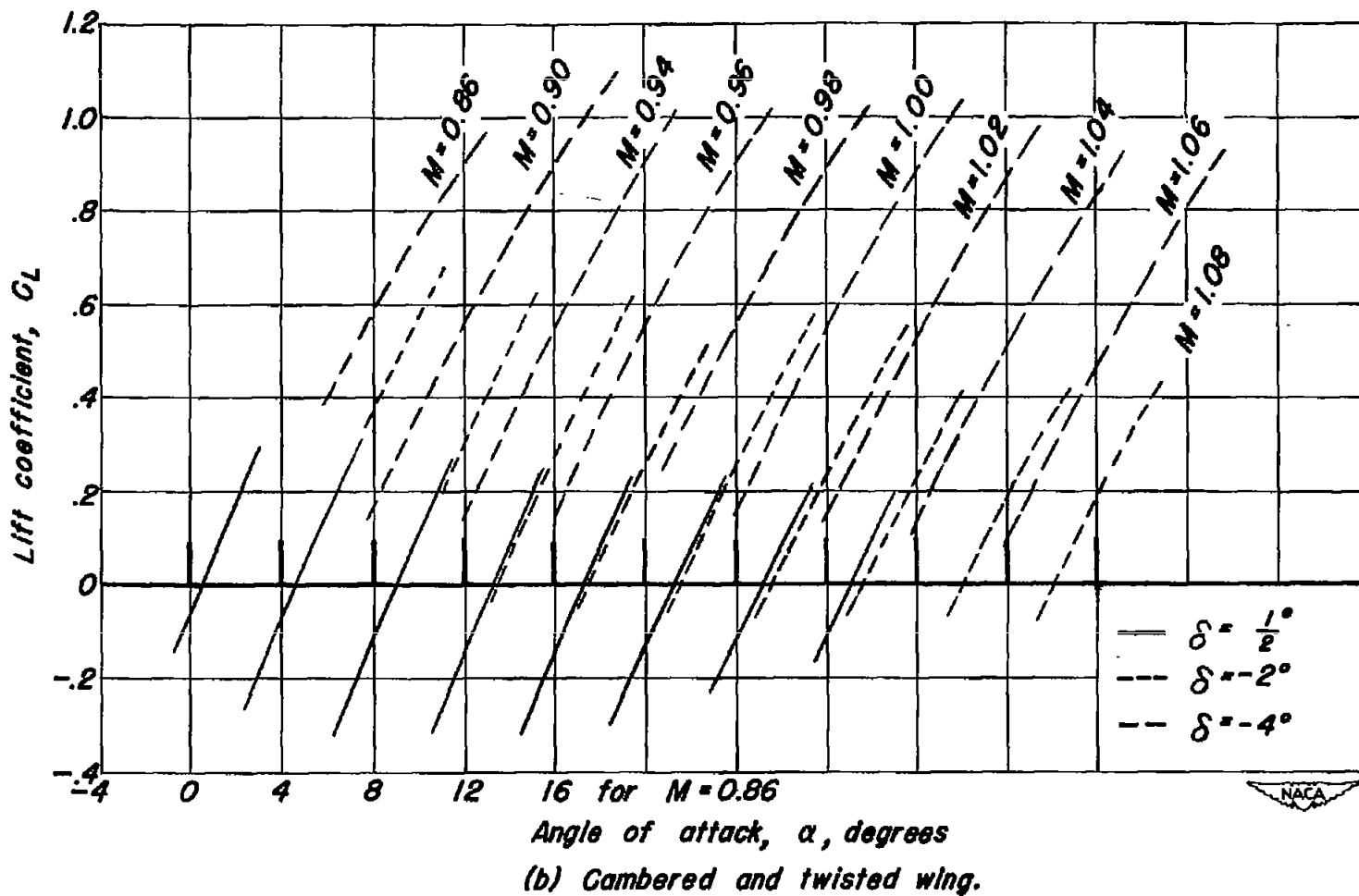


Figure 11.- Concluded.

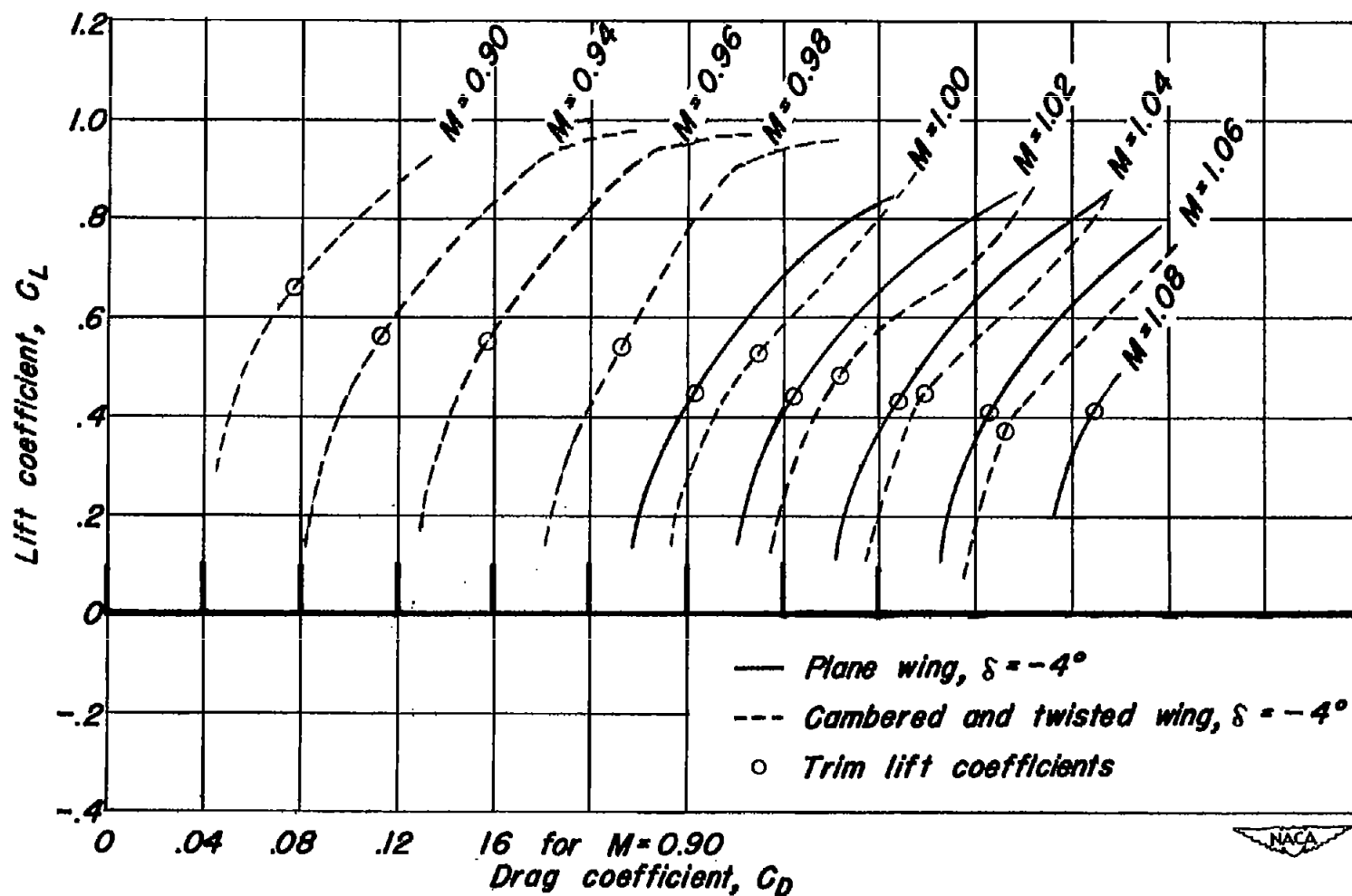
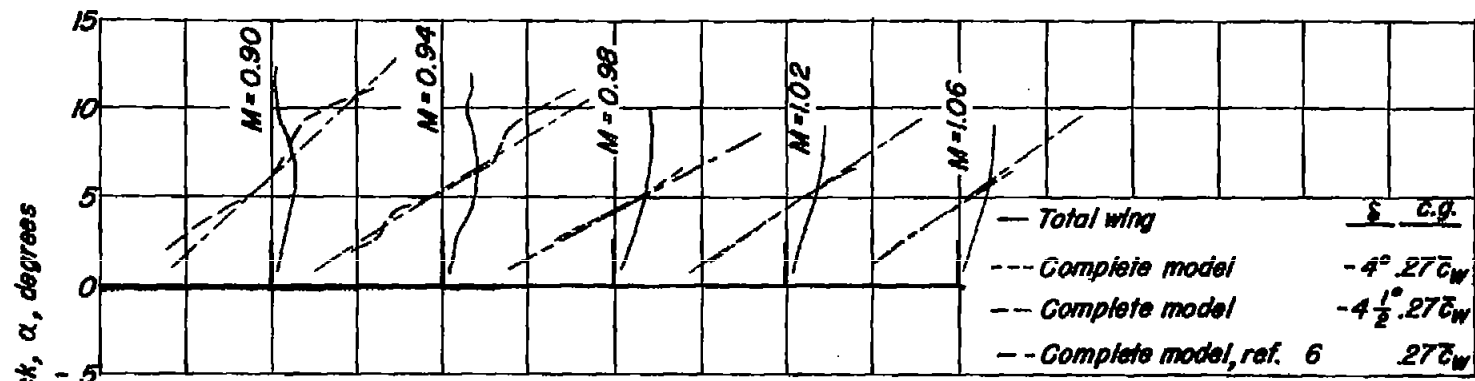
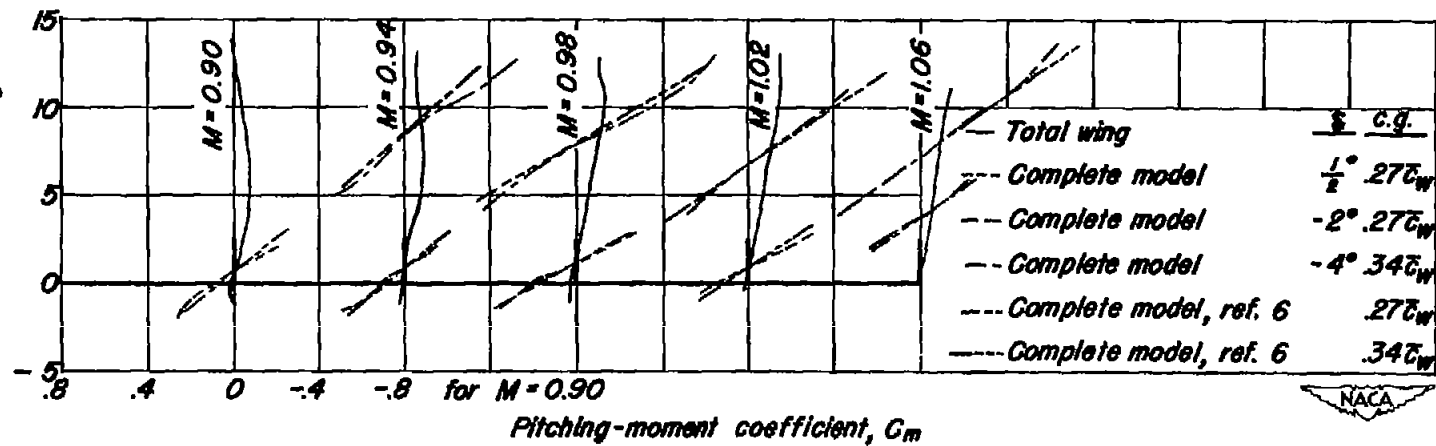


Figure 12.— The drag coefficients of the complete model at various Mach numbers, for the same stabilizer setting ( $\delta$ ) and the same fuselage (Model II).



(a) Plane wing.



(b) Cambered and twisted wing.

Figure 13.— The pitching-moment characteristics about the model center of gravity (c.g.) for the total wing and complete model at various Mach numbers, for different stabilizer settings,  $\delta$ .

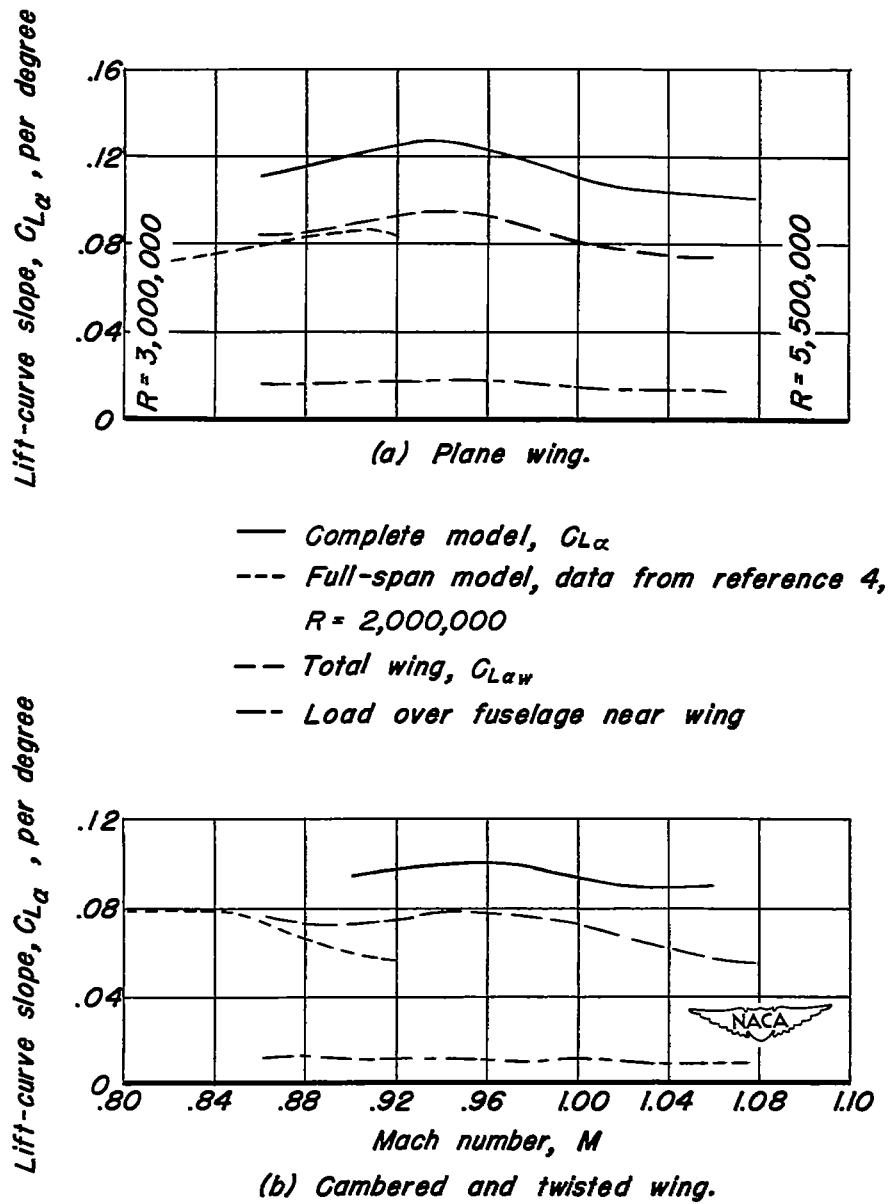


Figure 14.— Comparison of the lift-curve slopes of the two wings obtained from free-fall data with tunnel data from reference 4 (a for  $C_{Lw}$  is equal to 0.4).

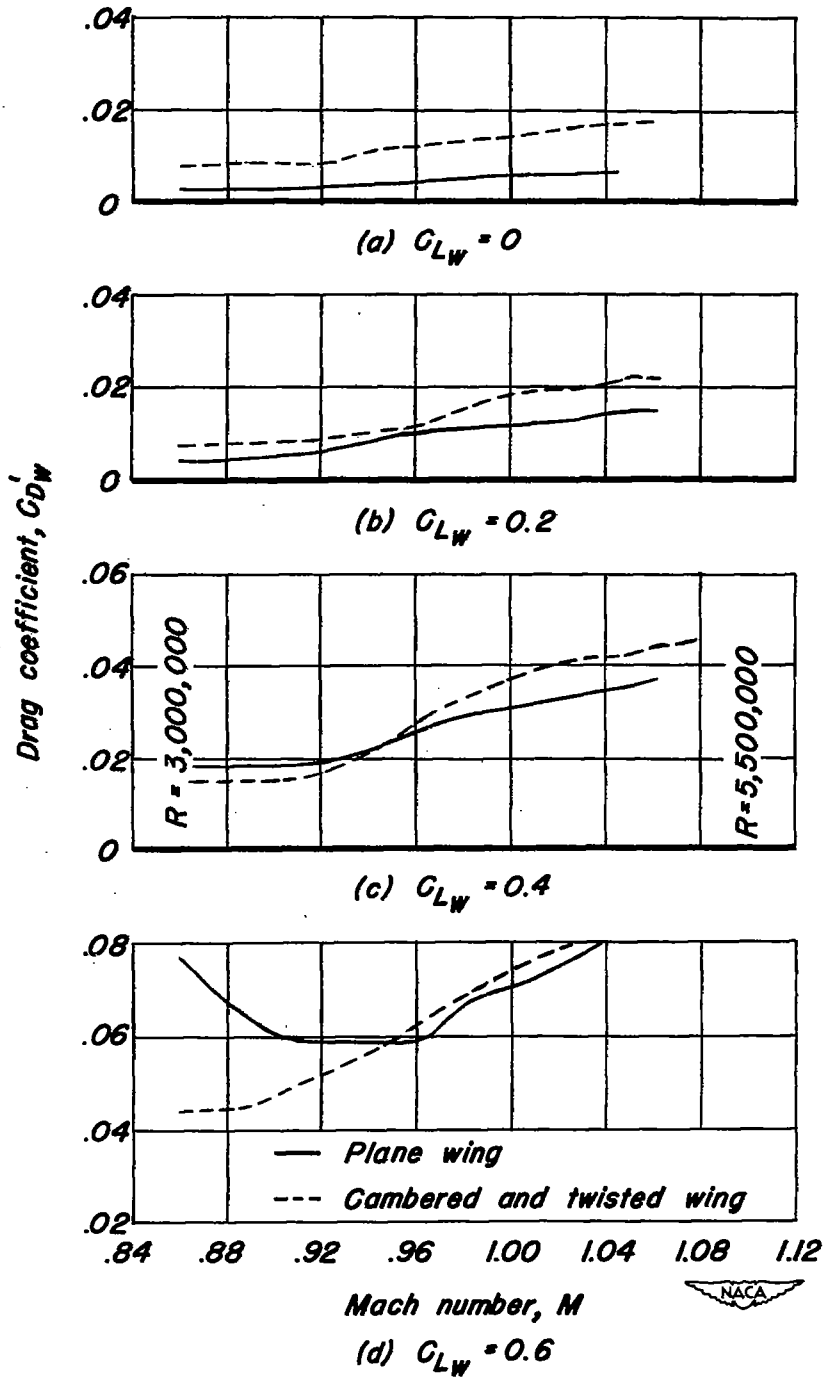


Figure 15.— The effect of Mach number on the drag characteristics of the two wings at various lift coefficients.

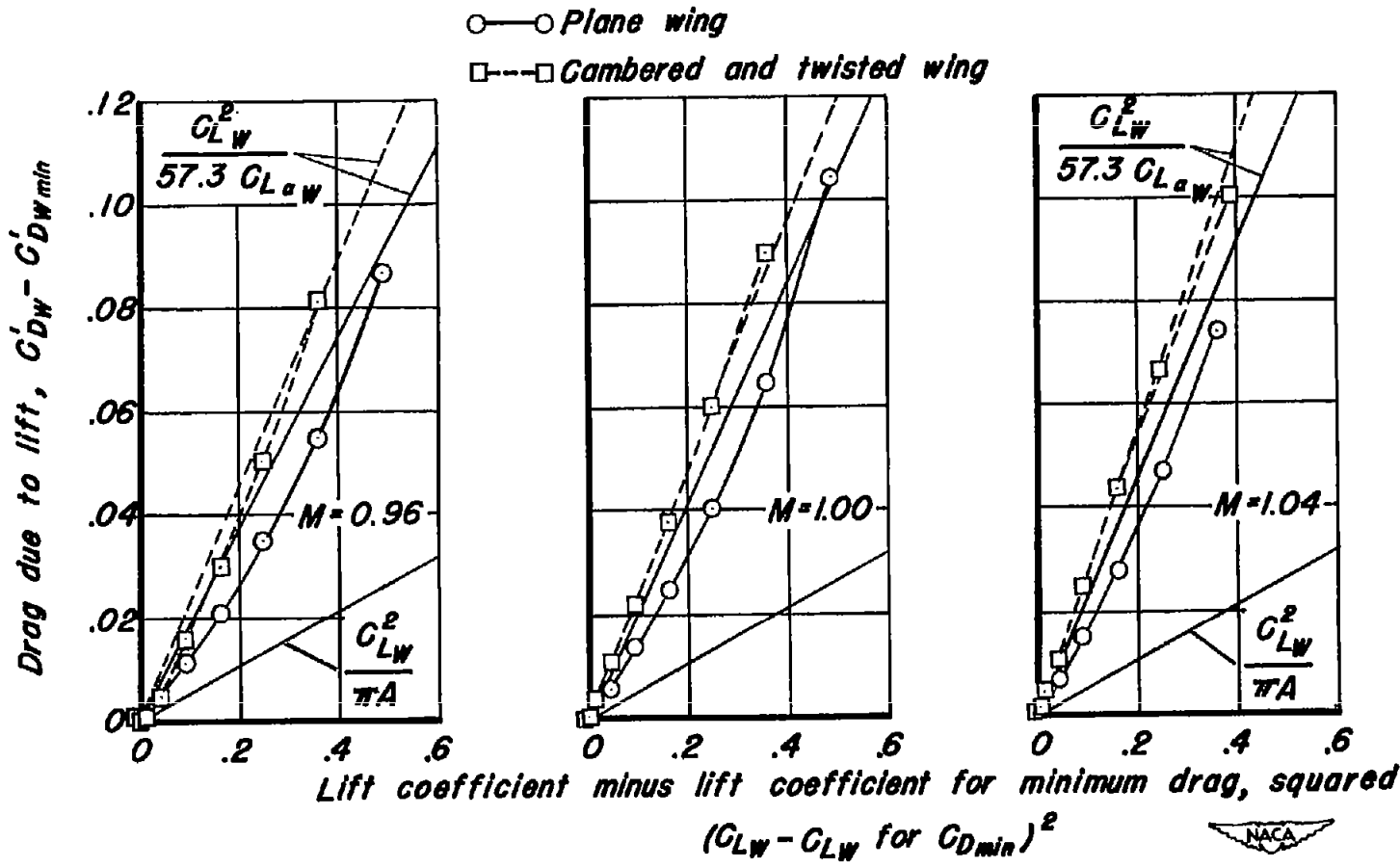


Figure 16.— Comparison of the drag due to lift for the two wings at several transonic Mach numbers with calculated slopes for full leading-edge suction ( $C_{LW}^2/\pi A$ ) and no leading-edge suction ( $C_{LW}^2/57.3 C_{L_{aW}}$ ).

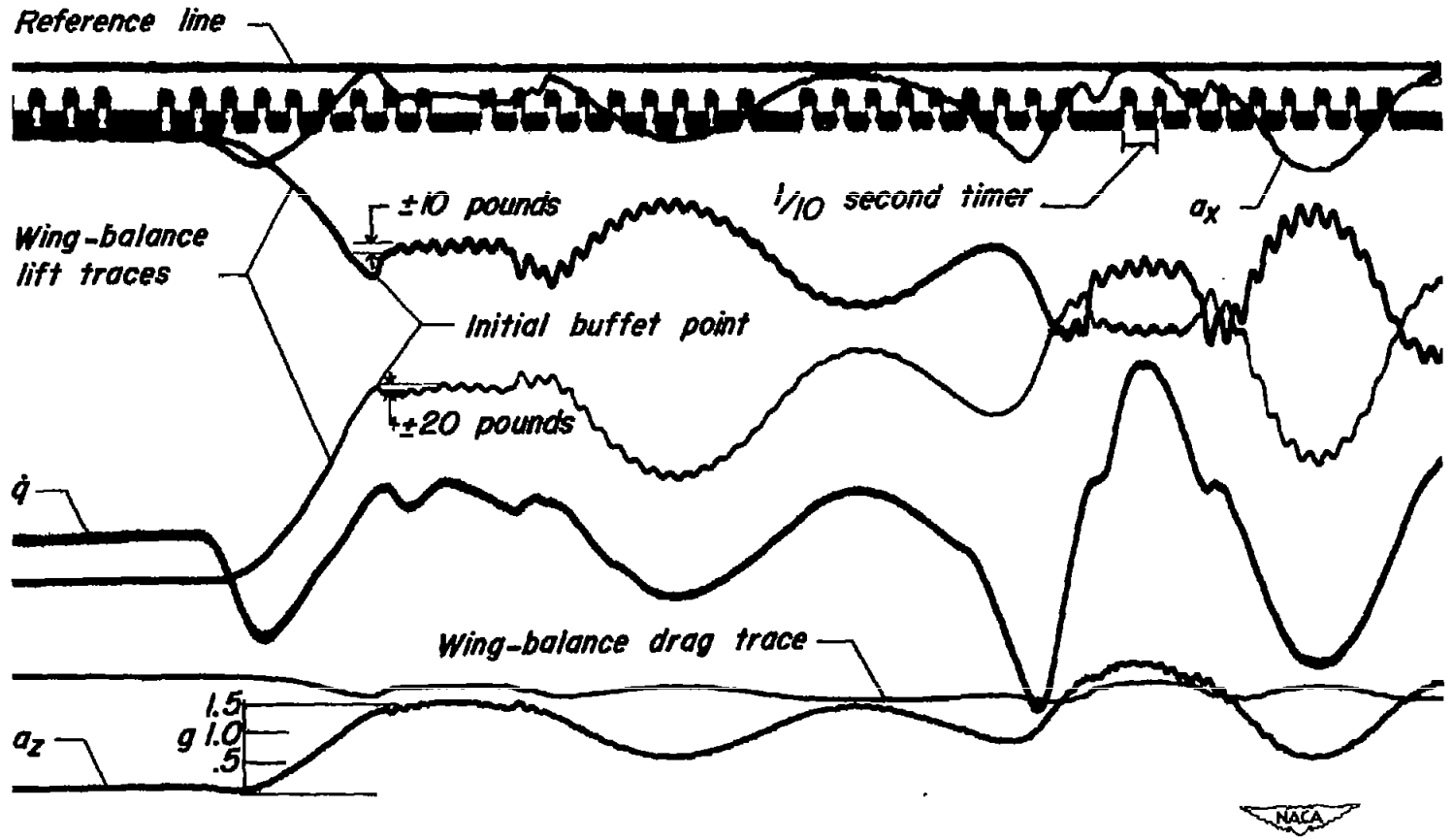


Figure 17.- Typical oscillograph record.

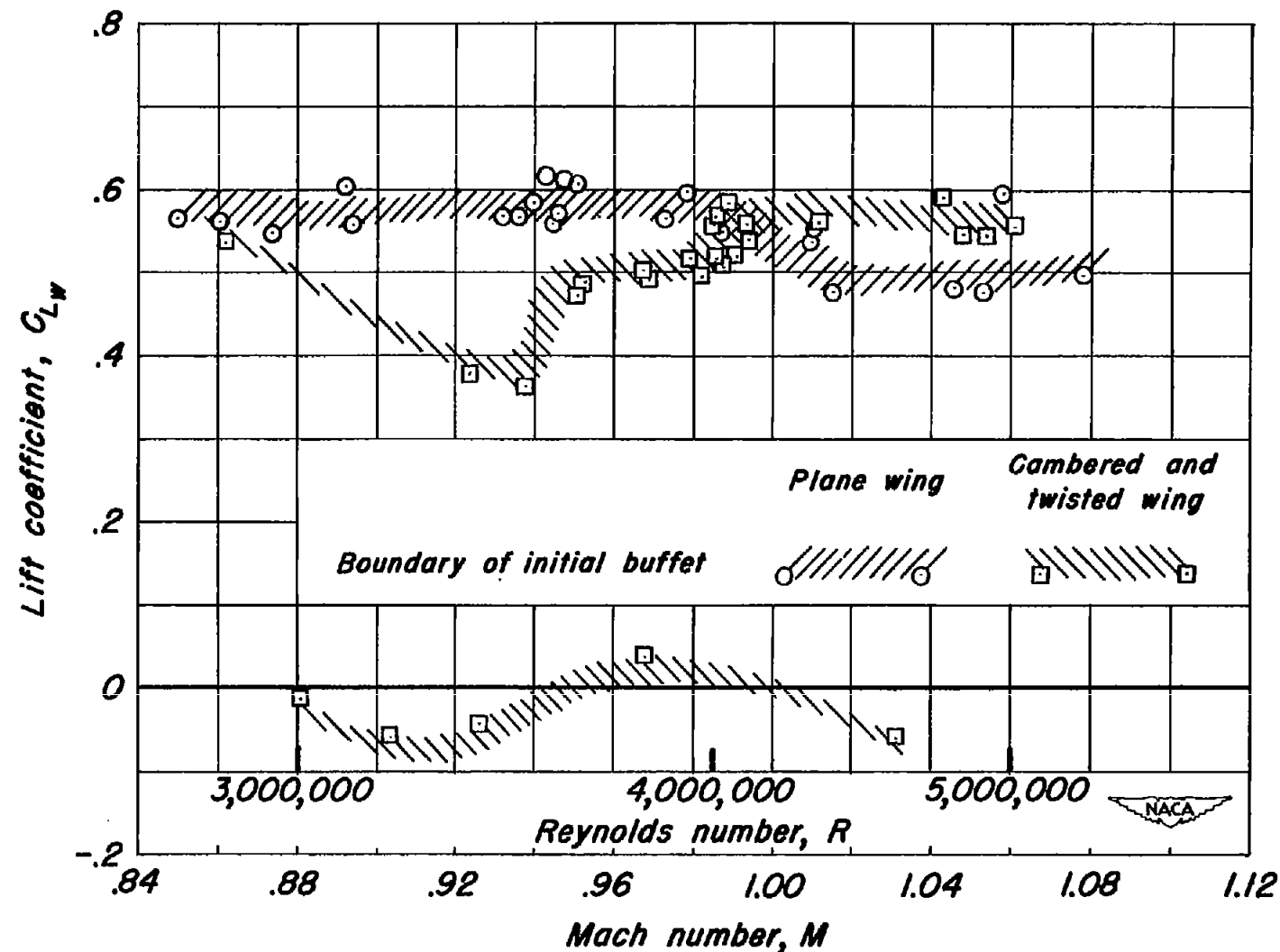


Figure 18.— Variation of the buffet boundaries with Mach number as indicated by the wing-balance records.

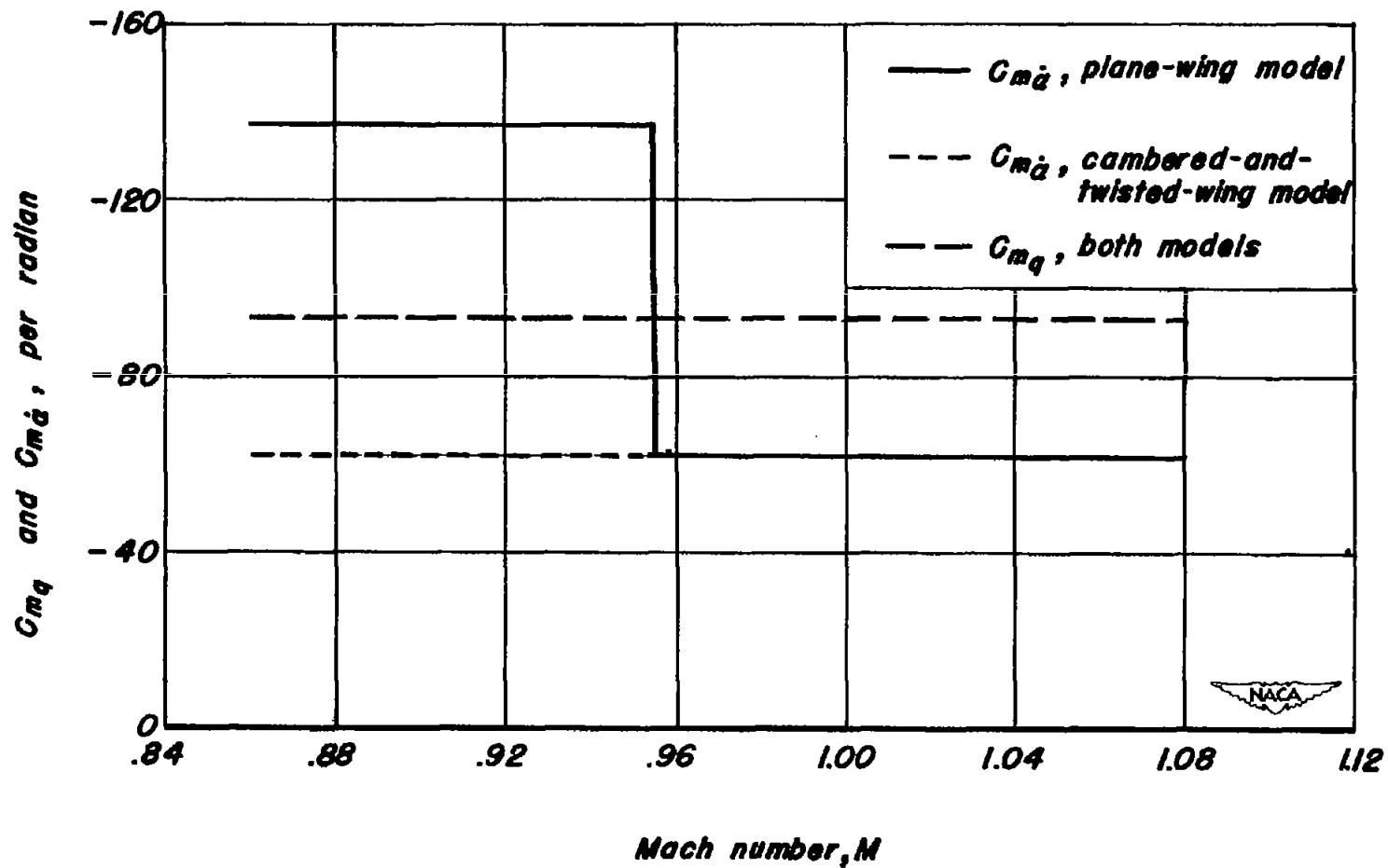
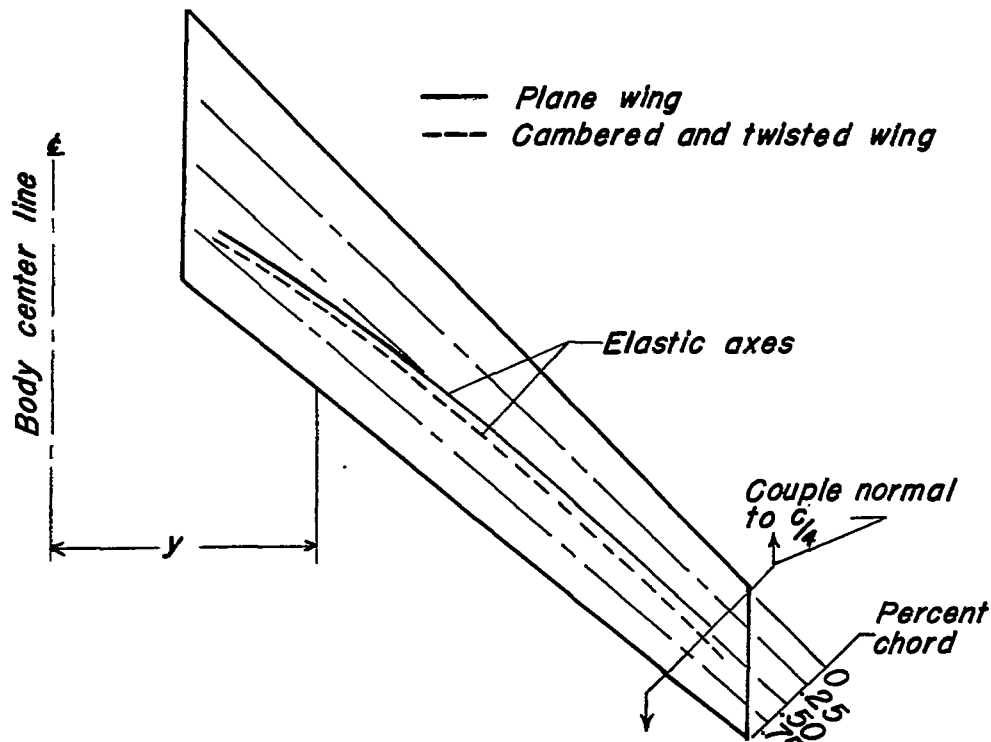
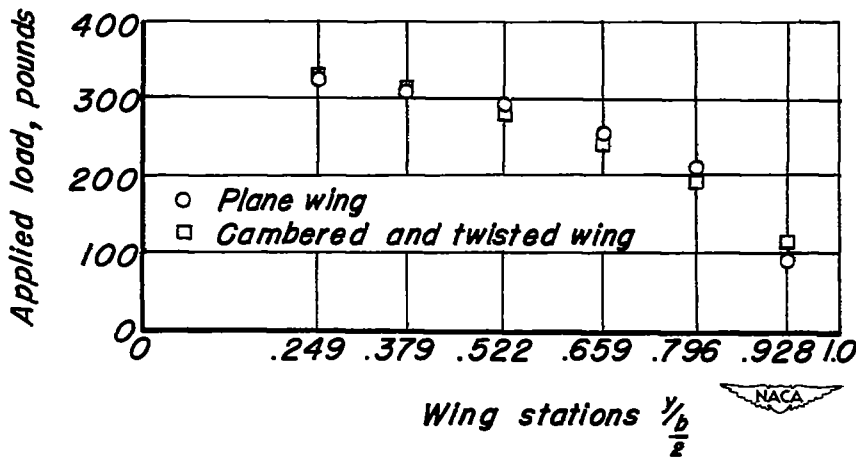


Figure 19.— Variation of  $C_{m_q}$  and  $C_{m_{\dot{\alpha}}}$  with Mach number as estimated by an approximate separation of the values of  $(C_{m_q} + C_{m_{\dot{\alpha}}})$  given in reference 6.



(a) Elastic axes as determined from couples applied at wing tip.



(b) Distribution of loads applied along the elastic axes to determine wing deflections in bending.

Figure 20.—Elastic axes and load distributions used to determine wing deflections in torsion and bending.

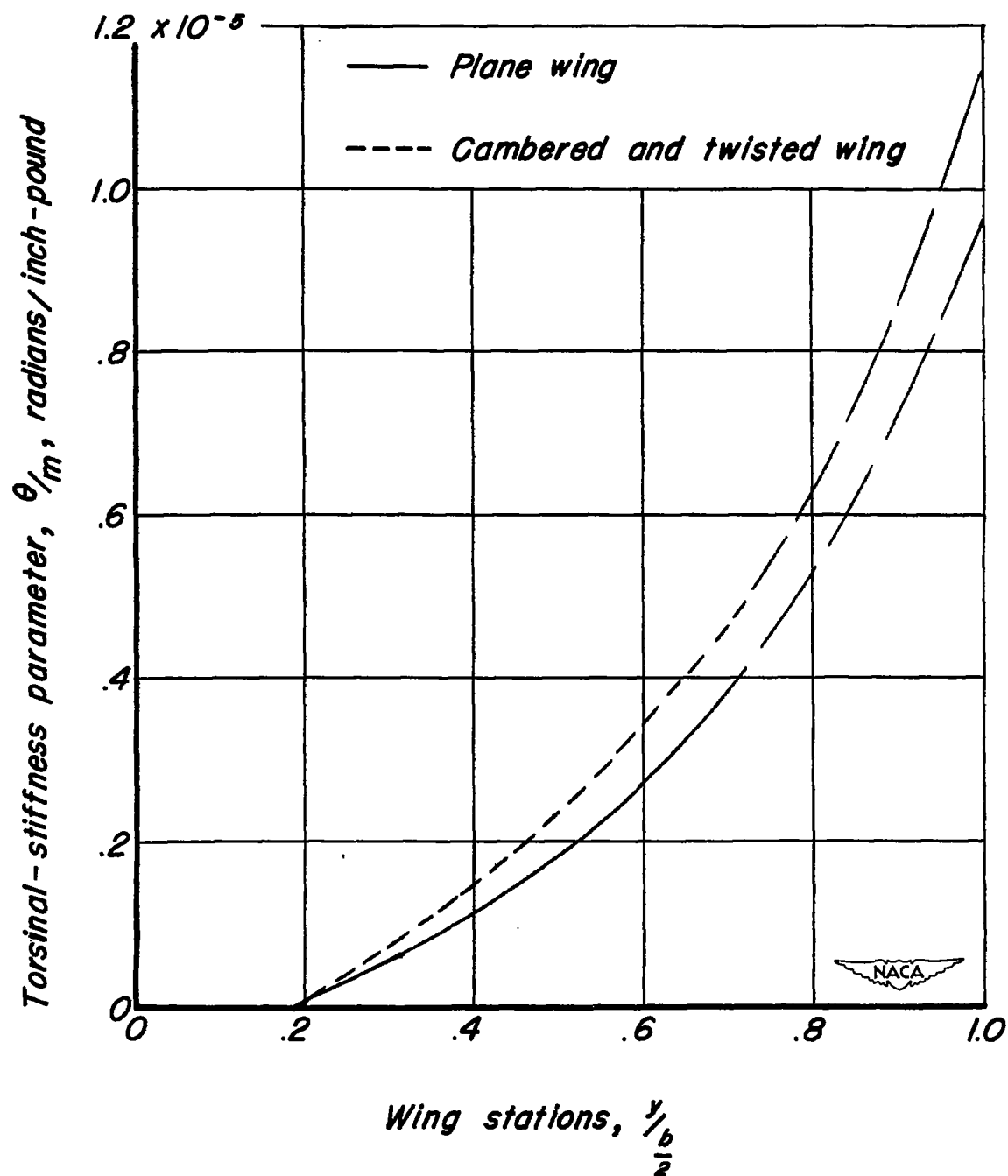


Figure 21.— Wing twist due to couples applied normal to to the quarter chord at the wing tip.

~~CONFIDENTIAL~~

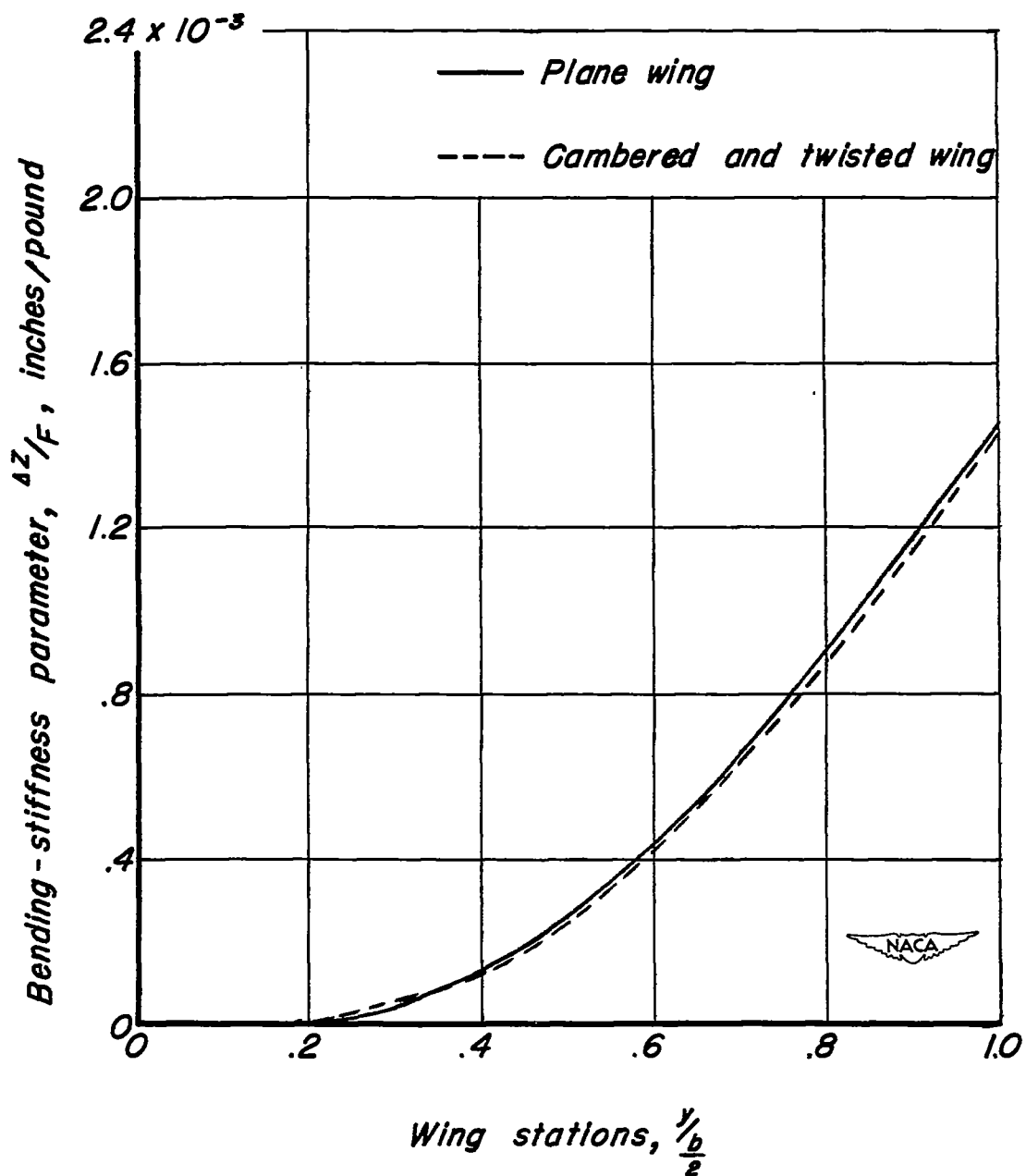


Figure 22.— Wing deflections ( $\Delta Z$ ) resulting from the application of a load ( $F$ ) distributed along the elastic axis. Curves presented represent averages of deflections for  $F$  equal to 500, 1000, and 1500 pounds.

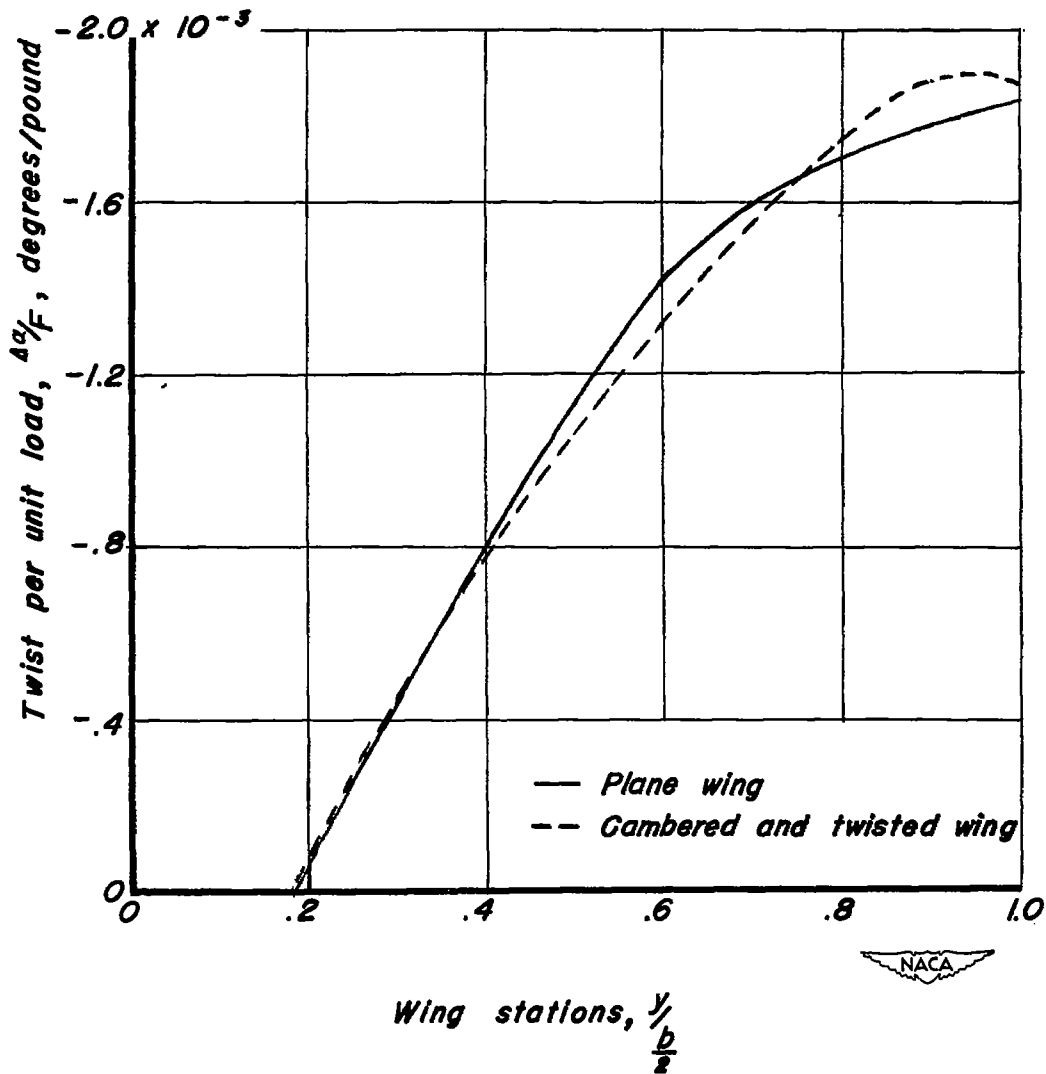


Figure 23.— Change in angle of attack ( $\Delta\alpha$ ) at any wing station resulting from the application of a load ( $F$ ) distributed along the elastic axis. Curves based on deflections presented in figure 22.

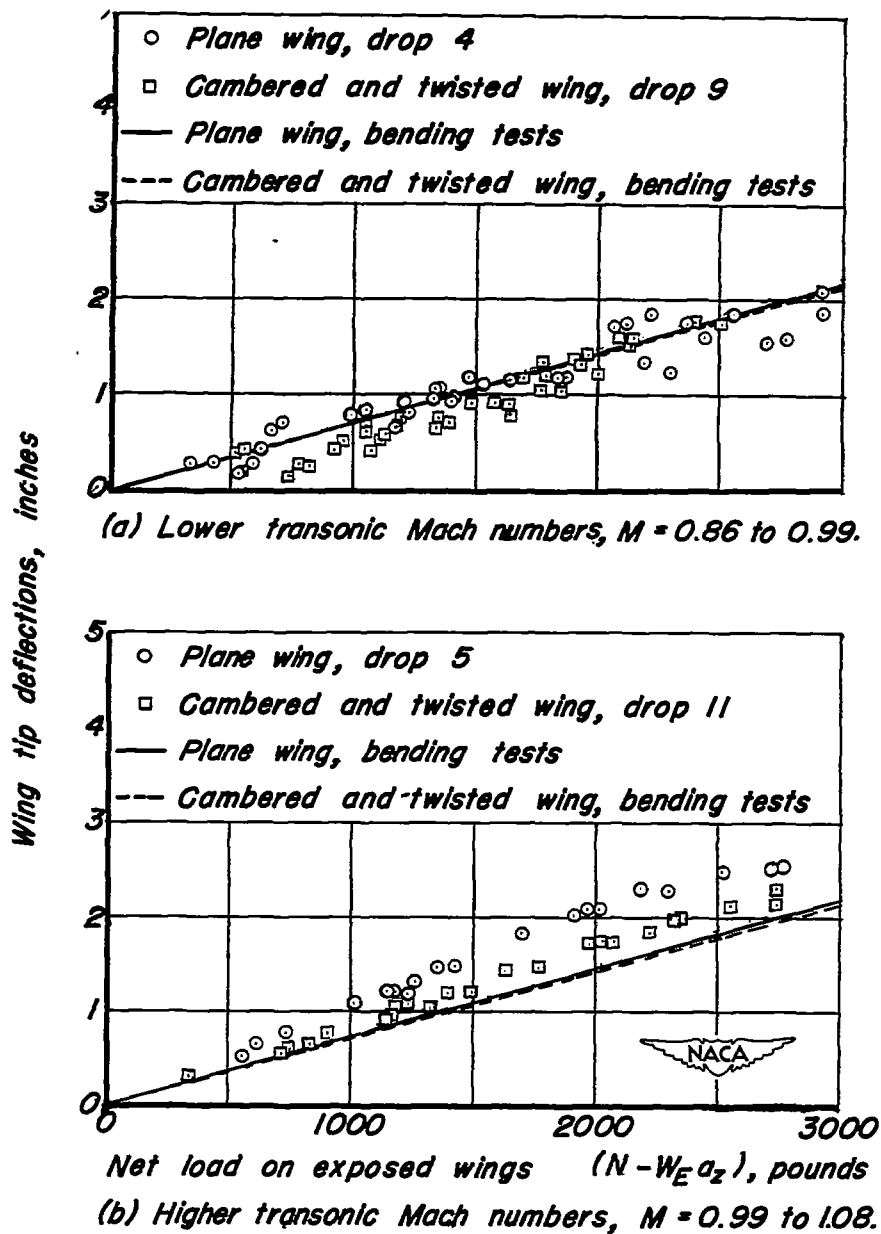


Figure 24. — Comparison between flight wing-tip deflections and deflections from bending using an applied spanwise load distribution based upon subsonic tunnel tests at  $C_L$  equal to 0.8 (reference 2).

CONFIDENTIAL